

**Subcellular Mechanics Regulates Structure and Function
of Neonatal and Stem Cell Derived Cardiomyocytes**

BY

Elina Sarmah

B.S., Georgia Institute of Technology, 2013

THESIS

Submitted as partial fulfillment of the requirements
for the degree of Master of Science in Bioengineering
in the Graduate College of the
University of Illinois at Chicago, 2015

Chicago, Illinois

Defense Committee:

Brenda Russell, Chair and Advisor

R. John Solaro, Physiology and Biophysics

Jun Cheng, Bioengineering

DEDICATION

This thesis is dedicated to my parents, for their endless love, support, and encouragement. Thank you both for teaching me to always be curious, and for giving me the strength to reach for the stars and chase my dreams.

ACKNOWLEDGMENTS

I would first like to thank my advisor and mentor, Dr. Brenda Russell, for your inspirational and timely advice and constant encouragement. During my time as a Master's student researcher, I have learned a great deal from your unique perspective on research, and I am humbly grateful for the honor to work with you and contribute to the lab.

Thank you Dr. R. John Solaro, Dr. Jun Cheng, and Dr. Brenda Russell for serving on my Master's Committee. I am truly grateful for your time and commitment towards my success.

Thank you to all the current and former members of the Russell Lab, including, Jieli (Shirley) Li, Mike Mkrtshjan, Ying-Hsi (Alvin) Lin, Kathleen Broughton, and Golnar Doroudian. Thank you for all the guidance and insights provided for my research. It was a pleasure to get to know all of you.

Thank you to the RRC Imaging Core Facility with Peter Toth, Ke Ma, and Tulika Sarma for always offering a helpful hand with conducting my confocal experiments.

Lastly, I would like to wholeheartedly thank my family: my parents, Rajib and Bandana Sarmah, and my sister, Raina Sarmah for their constant love and encouragement. Thank you for always staying by my side and motivating me to pursue my goals.

TABLE OF CONTENTS

	Page
I. Introduction	1
A. Cardiac Physiology	1
i. Heart Failure and Myocardial Infarction	1
ii. Physiology of the Heart	1
iii. The Sarcomere	5
iv. Mechanotransduction	6
v. Actin Assembly	7
B. Bioengineering Techniques	9
i. Cellular Biomechanics	9
ii. Biomimetic Materials and Devices	11
C. Stem Cells in Research	14
i. Human-Induced Pluripotent Stem Cells	14
ii. Human Cardiomyopathy from Genetic Mutation	16
 II. Subcellular Contractility and Actin Assembly as Influenced by 3D Microtopography in Neonatal Rat Ventricular Myocytes	 19
A. Overview	19
B. Materials and Methods	19
i. Fabrication of BioMEMS Substrates	19
ii. Substrate Stiffness	20
iii. Substrate Preparation for Cell Culture	20
iv. NRVM Culture	21
v. Immunohistochemistry	21
vi. Fluorescent Confocal Microscopy	22
vii. Measuring Shortening and Shortening Velocity	22
viii. Actin FRAP Dynamics	25
ix. Analysis of Fluorescence Recovery after Photobleaching	25
x. Statistical Analysis	26
C. Results	27
i. Substrate Stiffness	27
ii. Cell Structure Influence from Microposts	27
iii. Shortening and Shortening Velocity as a Function of Distance from Micropost	27
iv. Actin FRAP Dynamics as a Function of Distance from Micropost	30
v. PKC- ϵ Concentration Near Micropost	30
D. Discussion	35
E. Conclusions	38

TABLE OF CONTENTS (continued)

III.	Sarcomere Structure and Assembly in Normal Human and cTnT Mutation Cardiomyocytes Derived from Induced Pluripotent Stem Cells	Page 39
A.	Overview	39
B.	Materials and Methods	39
i.	Substrate Fabrication	39
ii.	Substrate Preparation for Cell Culture	40
iii.	iPSC-CM Cell Culture	40
iv.	Real-time Phase Imaging	41
v.	Immunohistochemistry	42
vi.	Measuring Shortening and Shortening Velocity	42
vii.	Actin FRAP Dynamics	45
viii.	Analysis of Fluorescence Recovery after Photobleaching	45
ix.	Omecamtiv Mecarbil	46
x.	Statistical Analysis	46
C.	Results	47
i.	iPSC-CM Structure as a Function of Time after Replating	47
ii.	Beating Frequency	47
iii.	Shortening and Shortening Velocity of iPSC-CMs	47
iv.	Actin FRAP Dynamics in iPSC-CMs	53
v.	Effects of Omecamtiv Mecarbil at One Week after Plating	56
vi.	Effects of Omecamtiv Mecarbil at Two Weeks after Plating	56
vii.	Actin FRAP Dynamics in iPSC-CMs with Omecamtiv Mecarbil	57
D.	Discussion	64
E.	Conclusion	66
IV.	Conclusions	67
A.	Major Findings	67
B.	Significance	69
C.	Future Directions	69
V.	Cited Literature	70
VI.	Appendix	81
A.	Animal Care Approval Form	82
B.	Recombinant DNA Approval Form	83
C.	Curriculum Vitae	84

LIST OF FIGURES

1. Force-Velocity Curve
2. Schematic of Sarcomere
3. Micropost Array and Cell Anchorage
4. Substrate Stiffness Affects Cell Phenotype
5. Measuring Neonatal Rat Ventricular Myocyte Shortening, Shortening Velocity, and Beat Frequency using a Kymograph
6. NRVM Shortening Varies as a Function of the Distance from the 3D Micropost
7. NRVM Shortening Velocity Varies as a Function of Distance from the 3D Micropost
8. Actin-GFP Dynamics in NRVM
9. Actin Dynamics with 3D Attachment
10. Actin Dynamics as a Function of Distance from Micropost
11. PKC- ϵ Distribution as a Function of Distance from the 3D Micropost
12. Measuring Shortening, Shortening Velocity, and Beat Frequency in iPSC-CMs using a Kymograph
13. iPSC-CM Maturation at Week 1 in Normal and cTnT R173W Mutation Cells
14. iPSC -CM Maturation at Week 2 in Normal and cTnT R173W Mutation Cells
15. Normal and Mutation iPSC-CMs have Similar Beating Rates by Week 2
16. Maximum Shortening of Normal and Mutation iPSC-CMs is Similar
by Two Weeks
17. Maximum Shortening Velocity of Normal and Mutation iPSC-CMs as a Function of
Maturation
18. iPSC-CM infected with Actin-GFP for FRAP Experiments

19. Actin FRAP Dynamics in Mutation iPSC-CMs are Different at Week 1, but Similar to Normal iPSC-CMs by Week 2
20. Normal and Mutation iPSC-CMs Beats per Minute are not Significant Different when Treated with 200 nM Omecamtiv Mecarbil at Week 1
21. Normal and Mutation human iPSC-CMs Shortening Properties are not Significantly Different when Acutely and Continuously Treated with 200 nM Omecamtiv Mecarbil at Week 1
22. Normal and Mutation human iPSC-CMs Shortening Velocity are not Significantly Different when Acutely and Continuously Treated with 200 nM Omecamtiv Mecarbil at Week 1
23. Normal and Mutation human iPSC-CMs Shortening Properties are not Significantly Different when Acutely and Continuously Treated with 200 nM Omecamtiv Mecarbil at Week 2
24. Normal and Mutation human iPSC-CMs Shortening Velocity is Decreased with Acute and Continuous Treatments of 200 nM Omecamtiv Mecarbil at Week 2
25. Actin-FRAP Dynamics in Normal and Mutation human iPSC-CMs when Treated with 200 nM Omecamtiv Mecarbil

LIST OF ABBREVIATIONS

3D	Three Dimensions
ADP	Adenosine Diphosphate
AFM	Atomic Force Microscopy
APTES	3-aminopropyltrimethoxysilane
ATP	Adenosine Triphosphate
BPM	Beats Per Minute
BSA	Bovine Serum Albumin
CO	Cardiac Output
DAPI	4',6-diamidino-2-phenylindole
DCM	Dilated Cardiomyopathy
DMEM	Dulbecco's modified Eagle's medium
DMEM/F-12	Dulbecco's modified Eagle's medium
ECM	Extracellular Matrix
EDV	End-diastolic Volume
ESV	End-systolic Volume
FRAP	Fluorescent Recovery After Photobleaching
GFP	Green Fluorescent Protein
HCM	Hypertrophic Cardiomyopathy
HR	Heart Rate
iPSC	Induced Pluripotent Stem Cell
iPSC-CMs	Cardiomyocyte-derived Induced Pluripotent Stem Cell
LV	Left Ventricle

MI	Myocardial Infarction
NRVM	Neonatal Rat Ventricular Myocyte
P	Phosphate
PBS	Phosphate-buffered Saline
PC-1	Chemically defined, Serum-free Medium for Primary Cells
PDMS	Polydimethylsiloxane
Pi	Inorganic Phosphate
PKC- ϵ	Protein Kinase C- Epsilon
ROI	Region of Interest
RPMI	Roswell Park Memorial Institute Medium
SV	Stroke Volume
TBST	Tris-buffered saline – Tween 20
Tm	Tropomyosin
TnC	Troponin C
TnI	Troponin I
TnT	Troponin T

SUMMARY

According to the American Heart Association, approximately one-third of deaths in the US are caused by cardiovascular disease (Mozaffarian et al. 2015). During cardiovascular disease conditions, such as myocardial infarction (MI), the heart changes in size, shape, and performance in response to altered functional demands - a process known as “remodeling”. The use of bioengineering techniques to fabricate BioMEMS devices provides a model for studying cardiomyocyte mechanics under physiologically realistic conditions. Cardiomyocyte response to mechanical cues is commonly quantified by measuring its shortening, shortening velocity, and surface stress and tension. Applying different loads to these cells can vary their response at the subcellular level. To examine this variability, neonatal rat ventricular myocytes (NRVMs) were plated on 100 kPa PDMS substrates, attached to microposts. Line scan methods were used to measure the sarcomeric shortening and velocity differences along the length of a single cardiomyocyte. The area with the maximum shortening and velocity were greatest towards the centroid region of the cell ($0.65 \pm 0.29 \mu\text{m}$ at $1.78 \pm 0.30 \mu\text{m/s}$), lower in the region near the post ($0.94 \pm 0.107 \mu\text{m}$ at $2.82 \pm 0.17 \mu\text{m/s}$) ($p = 0.006$), and lowest in the region furthest from the post ($0.52 \pm 0.26 \mu\text{m}$ at $1.03 \pm 0.34 \mu\text{m/s}$) ($p < 0.001$).

To study the effect of static load on actin filament assembly, the dynamics of sarcomeric actin were measured through FRAP in NRVMs. The kinetic constant (K_{FRAP}) obtained from the results of the curve fitting was significantly greater in the cell region near to the post ($6.45 \times 10^{-4} \text{ sec}^{-1} \pm 1.4 \times 10^{-4}$) than the mid-region of the cell ($3.89 \times 10^{-4} \text{ sec}^{-1} \pm 1.4 \times 10^{-4}$) ($p = 0.038$) and the region furthest from the cell ($1.91 \times 10^{-4} \text{ sec}^{-1} \pm 7.8 \times 10^{-5}$) ($p = 0.048$).

The use of these bioengineering techniques was also applied towards stem cells for potential use for drug discovery. Human induced pluripotent stem cell derived cardiomyocytes

(iPSC-CMs) provided a model for studying cardiac disease and therapeutic treatments. In this study, iPSC-CMs were derived from a family possessing a cardiac troponin T point mutation, which causes dilated cardiomyopathy. These cells (normal and mutant) were plated on 100 kPa PDMS substrates to mimic heart tissue stiffness. Immunohistochemistry images showed that the normal iPSC-CMs were more mature in terms of sarcomere development than the mutant cells. At Week 1 after plating, the shortening was higher in the normal group $0.88 \pm 0.04 \mu\text{m}$ (n=41) than in the mutation group $0.47 \pm 0.03 \mu\text{m}$ (n=36) μm in the mutation group ($p < .0001$). Similarly with the velocity, at week 1 it was $2.06 \pm 0.10 \mu\text{m/s}$ for normal group (n=41), which was significantly higher than $0.93 \pm 0.12 \mu\text{m}$ (n=36) in the mutation ($p < .0001$). Actin dynamics also showed a higher kinetic constant (K_{FRAP}) value in normal cells $5.94 \times 10^{-4} \pm 0.0001$ (n=6) than in mutant cells $2.66 \times 10^{-4} \pm 3.78 \times 10^{-4}$ (n=9) ($p=0.02$). By Week 2, the shortening and shortening velocity were not significantly different between normal and mutant cells. Shortening was 0.89 ± 0.05 (n=36) μm in the normal group, and $0.70 \pm 0.04 \mu\text{m}$ (n=44) in the mutation group. Shortening velocity was $1.91 \pm 0.065 \mu\text{m/s}$ (n=45) for normal, and $2.06 \pm 0.16 \mu\text{m/s}$ (n=44) for mutation. Actin FRAP dynamics in mutation cells reached the same range for normal cells by Week 2: (K_{FRAP}) values obtained were $3.73 \times 10^{-4} \pm 8 \times 10^{-5}$ (n=6) for normal and $4.04 \times 10^{-4} \pm 6.07 \times 10^{-5}$ (n=7) mutation.

To test the effects of the calcium-sensitizing drug, iPSC-CMs were treated acutely and chronically with 200 nM Omecamtiv Mecarbil, With an acute dosage of 200 nM Omecamtiv Mecarbil, the normal group BPM was 14.5 ± 1.1 (n=14) and the mutation group BPM was 14.6 ± 1.9 (n=9). The cells were also treated continuously, which resulted in a BPM of 11.4 ± 1.5 (n=14) for the normal group, and 11.6 ± 0.9 (n=8) for the mutation group At one week after plating, the normal cells showed a maximum shortening at $0.93 \pm 0.06 \mu\text{m}$ (n=12) compared to

the mutation at $0.42 \pm 0.04 \mu\text{m}$ (n=10) in the mutation group with an acute treatment. When a 200 nM dose of Omecamtiv Mecarbil was applied chronically, the maximum shortening was $0.96 \pm 0.04 \mu\text{m}$ (n=13) for normal, and $0.59 \pm 0.05 \mu\text{m}$ (n=9). The corresponding shortening velocities for the acute treatment were $1.72 \pm 0.14 \mu\text{m/s}$ (n=12) and $0.90 \pm 0.10 \mu\text{m/s}$ (n=10) for normal and mutation respectively. With the continuous treatment, the corresponding shortening velocities were $1.75 \pm 0.10 \mu\text{m/s}$ (n=13) and $1.24 \pm 0.11 \mu\text{m/s}$ (n=9) for normal and mutation, respectively.

At Week 2 after plating, iPSC-CMs were also treated with acutely and chronically with 200 nM Omecamtiv Mecarbil. With an acute treatment, the maximum shortening was calculated to be $1.14 \pm 0.06 \mu\text{m}$ (n=4) compared to the mutation at $0.74 \pm 0.11 \mu\text{m}$ (n=4) in the mutation group when treated acutely. When a 200 nM dose of Omecamtiv Mecarbil was applied chronically, the maximum shortening was $1.21 \pm 0.13 \mu\text{m}$ (n=3) for normal, and $0.85 \pm 0.15 \mu\text{m}$ (n=3). The corresponding shortening velocities for the acute treatment were $1.28 \pm 0.18 \mu\text{m/s}$ (n=4) and $4.10 \pm 0.33 \mu\text{m/s}$ (n=4) for normal and mutation respectively. With the continuous treatment, the corresponding shortening velocities were $1.95 \pm 0.27 \mu\text{m/s}$ (n=13) and $3.08 \pm 0.11 \mu\text{m/s}$ (n=3) for normal and mutation, respectively. The shortening velocity decreased in the normal iPSC-CMs when treated acutely ($p = 0.004$) and chronically ($p = 0.05$).

Actin FRAP dynamics were not affected by 200nM Omecamtiv Mecarbil At Week 1, the kinetic constant (K_{FRAP}) obtained from the results of the curve fitting was $6.38 \times 10^{-4} \pm 3.3 \times 10^{-5}$ (n=3). At Week 2, the kinetic constant (K_{FRAP}) obtained from the results of the curve fitting was $4.07 \times 10^{-4} \pm 8.30 \times 10^{-5}$ (n=2) for the normal group treated with Omecamtiv Mecarbil and the mutation group treated with Omecamtiv Mecarbil had an average K_{FRAP} value of $2.80 \times 10^{-4} \pm 5.6 \times 10^{-5}$ (n=4).

This study demonstrates useful tools and methods to mimic cardiac physiology for application in a complex, biomechanical system. Studying cardiomyocytes on 3D microtopography substrates provide a model that shows that contractility and actin assembly are regulated at the subdomain level. The use of human induced pluripotent stem cell derived cardiomyocytes offers a useful model for studying cardiac disease. Through this investigation it is shown that diseased cardiomyocytes derived from stem cells have lower functional properties as compared to normal stem-cell derived cardiomyocytes. Finally, the drug Omecamtiv Mecarbil provides insight into a potential treatment for heart failure and motivates further the further study of its effect on the diseased heart.

I. Introduction to Cardiac Physiology

A. Cardiac Physiology

i. Heart Failure and Myocardial Infarction

According to the American Heart Association, approximately one-third of deaths in the US are caused by cardiovascular disease (Mozaffarian et al. 2015). The cause of congestive heart failure is mostly due to ischemia, the restriction of blood flow to tissues (He 2001). During cardiovascular disease conditions such as myocardial infarction (MI), the heart changes in size, shape, and performance in response to altered functional demands - a process known as “remodeling”. Cardiac remodeling in severe disease occurs largely in the left ventricle of the heart, resulting in declining contractile (systolic) function and reduced stroke volume. Heart failure can be due to ischemia, arrhythmia, or genetic mutations. Ischemia occurs when blood supply is restricted to the tissues due to vessels closing, leading to cell death, because of a lack of oxygen and glucose necessary for cell metabolism. Arrhythmia affects the electrical circuits that link one myocyte to another. Genetic mutations can affect any cardiac protein and are the main cause of a serious heart conditions, such as cardiomyopathy.

ii. Physiology of the Heart

The heart is a muscular pump that circulates blood throughout the entire body (Katz 2010). In fact, the heart can be viewed as two pumps in series. The first pump consists of the right ventricle and the right atrium that pumps blood to the lungs, and the second pump consists of the left ventricle and left atrium, which pumps blood to the brain and body. Blood enters the right atrium from the superior and inferior cavae when low in oxygen from the systemic circulation and is then passed to the right ventricle. It is then pumped through the lungs, into the

pulmonary circulation to receive oxygen and release carbon dioxide. Oxygenated blood is returned to the left atrium, passed through the left ventricle, and pumped out of the aorta to the systemic circulation, where carbon dioxide is metabolized from oxygen. Veins are responsible for the transport of blood into the heart, while arteries transport it away from the heart. The backward flow of blood is prevented via the aortic and pulmonary valves, as well as the tricuspid and the bicuspid. Ventricles have stronger and thicker walls than the atria, and the left ventricle wall is thicker than the wall of the right ventricle because of the greater force required to pump blood through the systemic circulation.

Cardiac output (CO) is the volume of blood being pumped from the heart in one minute. It is the function of heart rate (HR) and the stroke volume (SV), or the volume being pumped by one ventricle with each heartbeat:

$$CO = HR * SV$$

Ejection fraction (EF) is related to stroke volume in that it is the fraction of blood ejected from the left ventricle during a contraction, known as the systole. Before the systole begins, the left ventricle is filled with blood to its capacity, which is known as the end diastolic volume (EDV), during the diastole. The end systolic volume (ESV) is the minimum capacity in which the left ventricle pumps blood to during systole. Therefore, cardiac output can also be represented as

$$CO = HR * (EDV - ESV)$$

The Frank-Starling law of the heart states that an increase of the end diastolic volume leads to an increase of the stroke volume of the heart, with all other factors remaining constant (Starling 1920). This increase of blood volume stretches the walls of the ventricles, which causes the heart muscle to contract more forcefully. Stroke volume can also increase in response to greater contractility during external work, or exercise. The force-velocity relationship can be

used to describe this external work and shortening velocity (Figure 1) (Katz, 1939; Brutsaert 1962). The larger the external load applied on the muscle, the slower the rate of shortening.

The heart consists of several different types of cells: smooth muscle cells, endothelial cells, fibroblasts, and myocytes. Action potentials (AP) spread from one heart cell to the next through gap junctions. The depolarization releases calcium which triggers muscle contraction. The impulses of action potentials begin in the right atrium at the sinoatrial node (SA node), which then spreads electrical activity to the atrioventricular node (AV node).

The cause of electrical activity in the cardiomyocyte is based in its depolarization in the cardiac action potential. The action potential travels to the different regions of the cell which causes voltage-gated calcium channels to open, causing an influx of calcium into the cytosol. Calcium ions combine with troponin C, a regulatory protein, in the troponin complex to allow for contraction, and separates from the protein to enable relaxation in the cardiac muscle. Troponin C is present on thin filaments containing actin of the sarcomere. Normally, tropomyosin blocks binding sites on the thin filament to myosin. However, when calcium binds to troponin C, an allosteric change occurs in the troponin protein, enabling tropomyosin to move by troponin T, and unblocks these actin-myosin cross-bridge binding sites. When the myosin head binds to actin, a power stroke is initiated. A sliding motion along the actin filament is created, caused by a splitting of adenosine triphosphate (ATP), and a contraction occurs (Huxley, 1969).

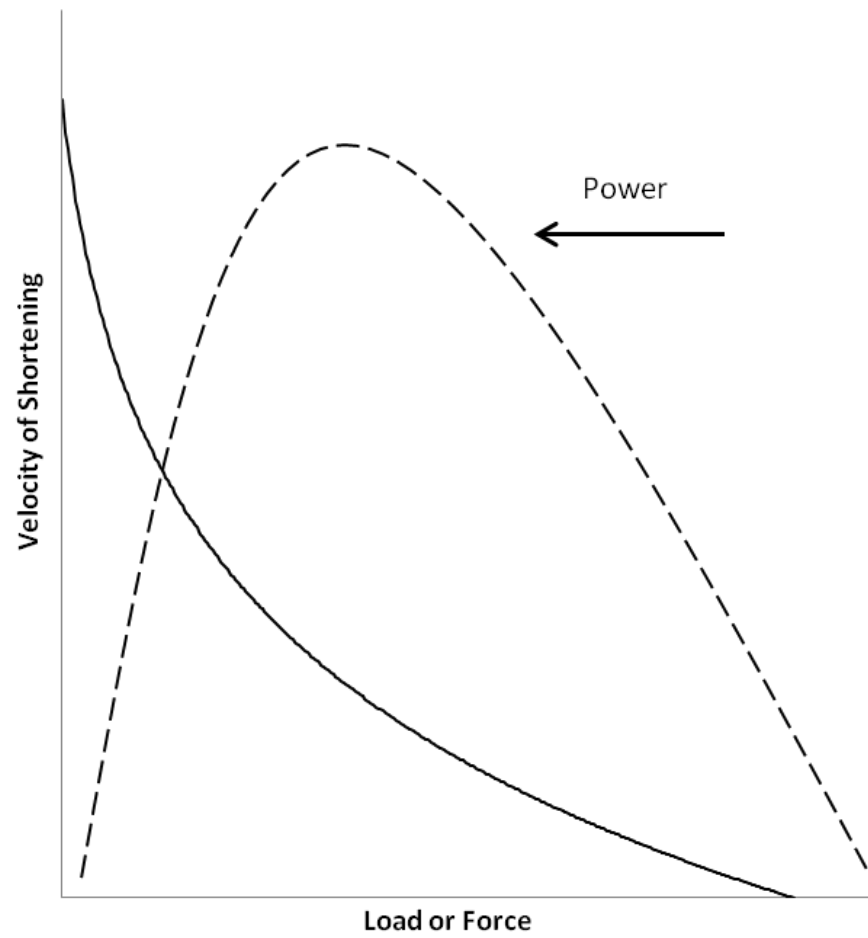


Figure 1: Force-Velocity Curve. The relationship between applied force and velocity in an isometric muscle, with the associated power

The power-stroke cycle describes the movement of myosin across the actin filament (Spudich 2001). It occurs with the hydrolysis of ATP and the release of energy (Hill 1968). First, ATP binds to myosin, which moves it to a high-energy state. When ATP is hydrolyzed by ATPase, it turns into ADP and inorganic phosphate (Pi). With this release of energy from ATP hydrolysis, the angle of the myosin head changes, which makes it ready to bind to actin when binding sites are open. Myosin is in a high-energy configuration, and ADP and Pi remain attached. Once the myosin binds to actin, Pi is released, and myosin returns to a lower energy state. When myosin expends this energy, it goes through a “power stroke” (Goody 2003). ADP is released after the power stroke, and the cross-bridge remains intact. Once ATP binds to myosin, and myosin moves the high-energy state, the myosin head is released from the active site on actin. This allows the cross-bridge cycle to start again. Without ATP, the muscle would remain contracted in rigor, rather than relaxed.

iii. The Sarcomere

Cardiomyocytes are essential for contractile function in order for the heart to pump blood through the body. They are composed of thick and thin filaments, comprised mainly of myosin and actin, respectively, and are organized within sarcomeres, the basic unit of muscle (Figure 2). Repeating bundles of sarcomeres are known as myofibrils. Myosin has a round, globular head and a long tail, and binds to actin. Actin molecules are bound to the Z-disk, which is one of the bands of the sarcomere and borders the edge of the sarcomere, and acts as an anchorage site for actin as well as titin, an elastic protein. Actin and titin are crosslinked via the protein alpha-actinin at the Z-disk. Surrounding the Z-disk is the I-band, which is the zone of thin filaments that does not overlap with thick filaments. Actin filaments are the major part of the I-band and

extend to the A-band. The A-band consists of the entirety of a single thick filament. Within this A-band is the H-zone, which is the region of thick filaments that does not overlap with thin filaments. Inside the H-zone is the M-line, which is the middle of the sarcomere, where actin and myosin overlap and interact. Here, titin also interacts with myosin, and is highly elastic in nature. It provides binding sites for several proteins and plays an important role in sarcomere assembly.

iv. Mechanotransduction

For attaching cells to the extracellular matrix (ECM), the focal adhesion complex is crucial (LaNaza 2009; Samarel 2005). This complex also connects the Z-disk to the membrane in order to regulate external and internal forces and signaling (Kaprielian 2000). The focal adhesion kinase (FAK), from which the focal adhesion complex is built on, induces a protein signaling pathway, which can also control cell motility (Mitra, 2005). Upon the maturation of the focal adhesion complex, it can serve as a region for force transmission within a cardiomyocyte.

Details of protein structures and functions within the cardiomyocyte are crucial for understanding mechanotransduction, a mechanism in which cells convert mechanical cues into biochemical responses. One such protein is the protein kinase C enzyme, which is encoded by the *PRKCE* gene in humans (Basta 1992). Protein kinase C, a serine / threonine kinase, was one of the earliest kinases to be discovered (Takai 1977). The PKC family has a numerous isoforms and several downstream substrates. It has shown to be important in the regulation of many cellular processes including survival, differentiation, proliferation, migration, and apoptosis. One isoform, PKC- ϵ , was first discovered among novel PKC isotypes by cDNA cloning. Today it is established that PKC- ϵ and PKC- δ , along with PKC- α , are the predominantly expressed PKCs in human and rodent hearts (Duquesnes 2011). PKC- ϵ has shown to enhance cardiac contractility

and remodeling (Deng 1997; Pi 2000). It also has a cardio-protective function in pre-conditioning the heart (Chen, 2001). An overexpression of PKC ϵ induces concentric cardiac hypertrophy (Takeishi, 2000). PKC- ϵ is translocated to the Z-disk when it is activated (Disatnik 1994; Dorn 1999; Robia, 2001). A dominant-negative mutant of PKC ϵ prevents the assembly of the optimal resting length of the sarcomere after sustained mechanical strain, suggesting a regulatory role in sarcomere assembly (Mansour, 2004).

v. *Actin Assembly*

Actin assembly is regulated by several protein complexes (Alberts, 2008). The assembly begins at the barbed ends of thin filament located in the Z-disk, regulated by formin, and the capping protein, CapZ. The formin protein family regulates assembly at the barbed ends (Pruyne 2002). Formin is functionalized by dimerization to become FH1 and FH2 that controls the actin elongation by wrapping around it. FHOD1 and FHOD3 are the domain-containing proteins of FH1 and FH2. FHOD3 contains two isoforms, the larger of which is located in the Z-disk, and is needed for maintenance of myofilaments.

In contrast, CapZ slows the process of actin polymerization. CapZ is a mushroom-shaped heterodimeric protein (Yamashita 2003). The C-terminus of both the α and β subunits of CapZ governs binding to actin. This protein helps in the stabilization of actin filaments, hence protecting it from assembling. Other regulatory proteins can induce this protein's activity by binding to actin filaments and blocking CapZ, thus allowing assembly.

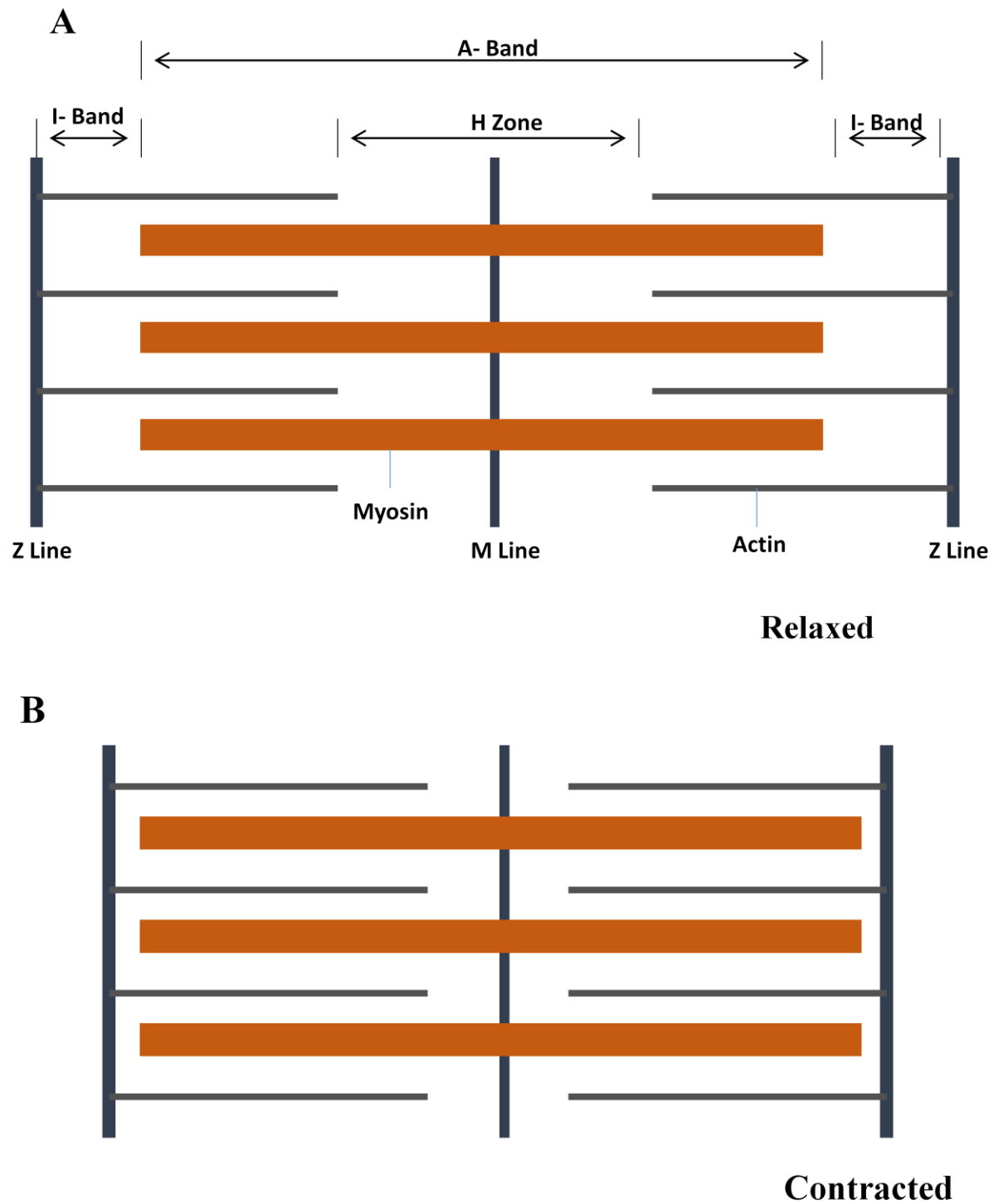


Figure 2: Schematic of Sarcomere. Different regions of the sarcomere are outlined when the heart is in its (A) relaxed state and (B) contracted state.

B. Bioengineering Techniques

i. Cellular Biomechanics

Several studies have been conducted to examine traction forces of live cells that sense mechanical cues and respond accordingly (Williams 1998, Ingber 2002). Advances in micropost fabrication technology have allowed for the quantification of mechano-transmission processes (Figure 3A). When cells, including cardiomyocytes, are plated on these microposts, they remodel over time with the most of their mass anchored against the post (Figure 3B) (Motlagh 2003; Broughton 2014). The nucleus of the cell also repositions closer to the post.

In static mechanics, microposts can be considered as vertical and cylindrical cantilever beams, with one end fixed to a surface, and the other end free (Cheng 2013). A force applied to the top end of the post can cause it to bend. The contractility pattern of a cell will alter the traction forces. Because of the flexibility of the materials used to create the microposts, cells attached to the posts can cause the post to bend. Changes in cell mechanical behavior are seen as the directional deflections of the posts are altered. In linear mechanics, a micropost can be seen as a spring, in that the deflection is directly proportional to the force being applied. A theory of cantilever beam bending, the Euler-Bernoulli Beam Theory relates post deflection (x) and force (F) for a cylindrical model:

$$x = \frac{64L^3}{3\pi ED^4} F = \frac{1}{k} F$$

where E is the Young's Modulus of the micropost, D and L are the diameter and deflection of the micropost, respectively. k is the spring constant of the micropost, which can be determined by using the size and Young's Modulus of the post. Cells that are anchored on a post tend to contract towards its physical center to counterbalance the forces on the array of microposts (Cheng 2010).

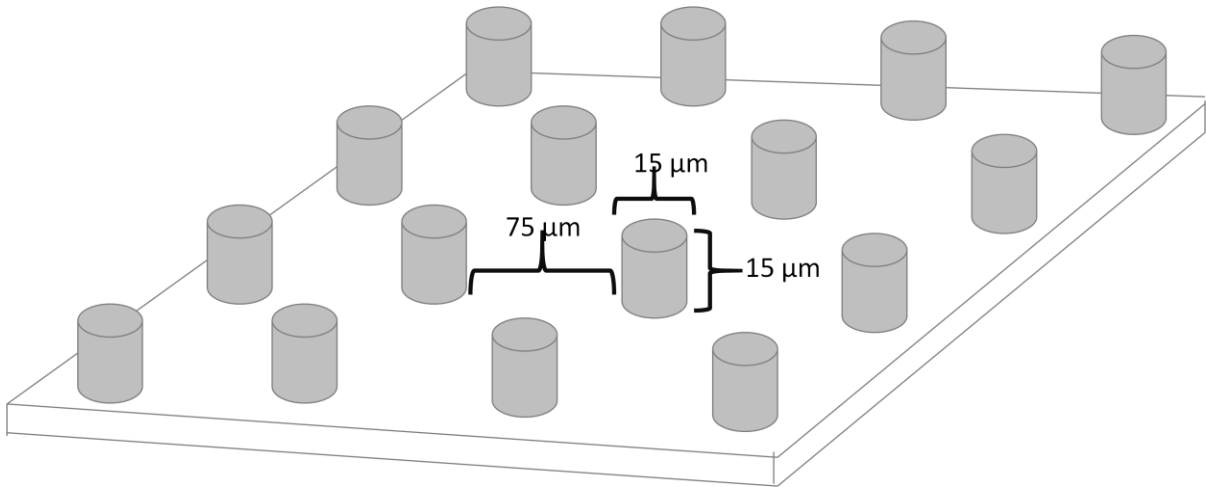
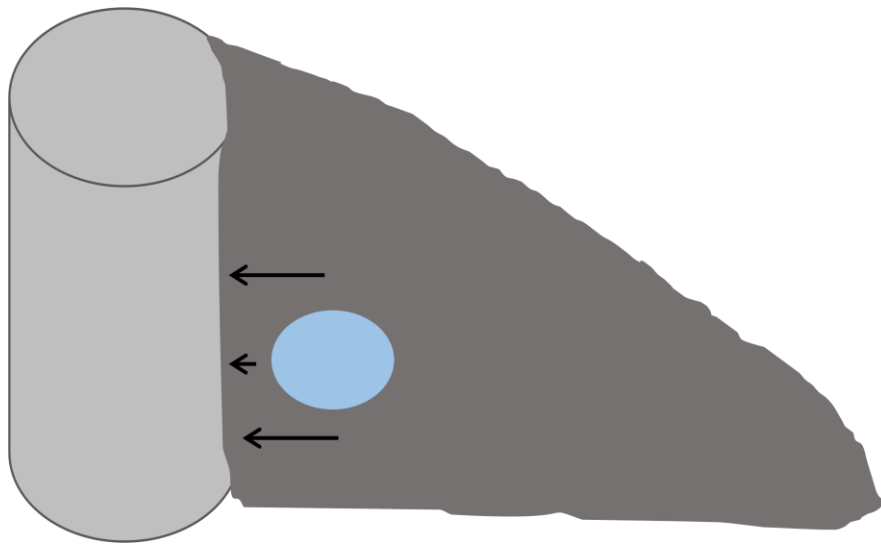
A**B**

Figure 3: Micropost Array and Cell Anchorage. (A) Schematic of tetragonal array of microposts that are $15\ \mu\text{m}$ high, $15\ \mu\text{m}$ in diameter, and spaced $75\ \mu\text{m}$ apart. (B) As the cell attaches itself to a micropost, the nucleus is also relocated near the post, and the cell applies a force onto the post to remain anchorage.

ii. *Biomimetic Materials and Devices*

To further understand the function the cells in vivo, simulated environments made on substrate surfaces in vitro are a key component in scientific research. This is because it has been well-researched that matrix stiffness and topography can induce a signaling cascade within a cell (Discher 2005; Engler 2008). The cell response to force generation can cause cellular remodeling.

The stiffness of the substrate material is dependent on the type of cell being studied (Discher 2005; Neimir 2010). Typically, the elastic modulus ranges of the surrounding cell tissue are 0.1 kPa-10 kPa for brain, 10 kPa- 500 kPa for adult cardiac muscle, 80 kPa - 50 MPa for skin, 300 kPa- 3 MPa for cartilage, and 10 MPa- 30 GPa for bone (Figure 4) (Discher 2005). Cells can sense the stiffness of the matrix, and the feedback of this stiffness on the cell state has a significant effect on development, differentiation, and regeneration (Discher 2005).

To create substrates at these varying stiffnesses, several biocompatible materials are considered. These materials include: polyacrylamide and poly(ethylene glycol) (PEG)-based, which are used to create hydrogels of softer stiffnesses (Pelham 1997; Flanagan 2002); polydimethylsiloxane (PDMS) and poly diacrylate (PEGDA), to create hydrogels to mimic stiffer tissues (Fuard 2008; Drumheller 1994). A material is chosen based on its ability to mold to a certain elastic modulus and mold into a 3D topographical textured surface in order to study advanced mechanotransduction.

To study the mechanics in cardiomyocytes, it is important to create microenvironments with specific topographical features in order to provide more insight on how they behave in their microenvironments. PDMS is a commonly used material to create such 3D microtextures, as it is also biocompatible, and easy to fabricate and use. The stiffness of PDMS can be tuned by using

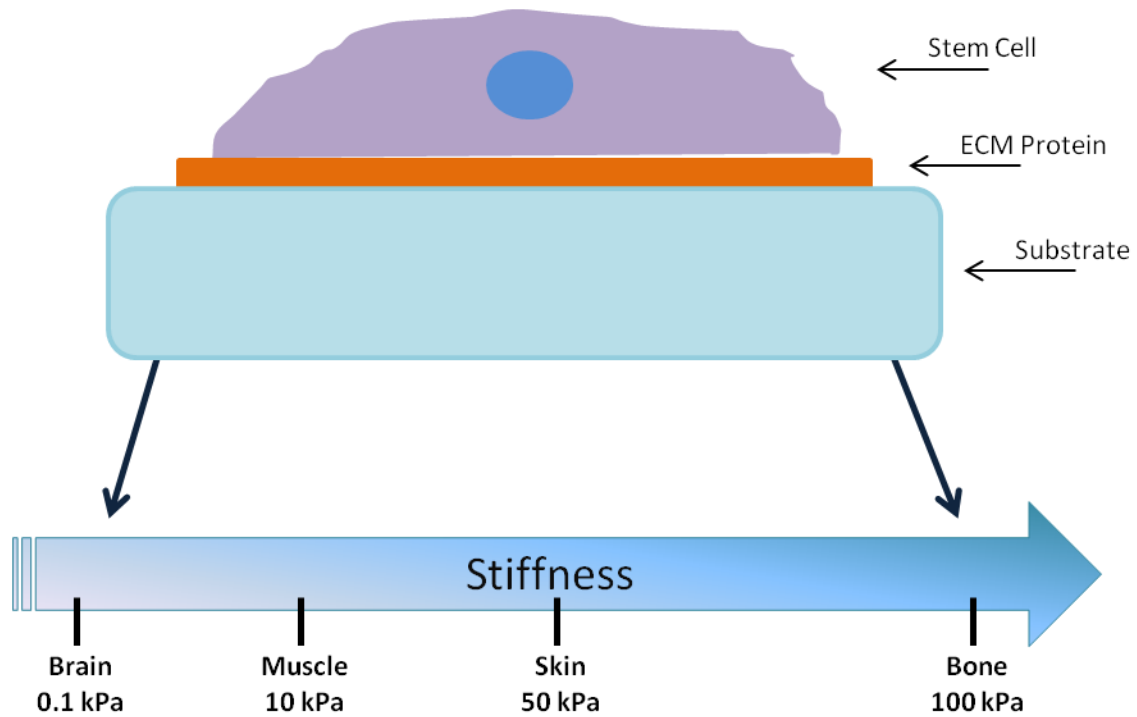


Figure 4: Substrate Stiffness affects Cell Phenotype. Cells are plated on substrates coated with an ECM protein for attachment. These substrates can be tuned to a range of stiffnesses depending on the cell type being studied.

different ratios of elastomer to curing agent at a particular temperature and time to crosslink the polymer chain (Hocheng 2010; Lee 2004). Atomic Force Microscopy (AFM) is used to confirm the material's stiffness by measuring the stress-strain relationship of the substrate. Using these processes, PDMS can successfully mimic the physiological conditions of the heart. The initial step to create the 3D microtopography of these environments is to mold their templates.

Photolithographic techniques are commonly used to create these templates (Motlagh 2003, Broughton 2014). The first step in the process is to spin a negative photoresist SU-8 2010 (Microchem, Newton, MA) at 1200 RPM for thirty seconds on a silicon wafer, 3 inches in width, which creates the photoresist depth of 15 μm . The wafers are then cured for five minutes at 95°C and aligned with a Karl Suss MJB3 mask and a patterned transparency mask. For this particular study, the transparency mask was patterned with 15 μm - diameter circles spaced 75 μm apart to create microposts. The wafer is then exposed to a light source (365 nm at 13 mW/cm²) for 30 seconds, and cured again for 10 minutes at 95°C. Any non-cross-linked photoresist is removed by placing the mask in a SU-8 developer (Microchem) for a minute.

To proceed with the next steps, the wafers are then transported to a parylene deposition system (PDS) 2010 Labcoater (SCS Coatings, Indianapolis, IN). The final parylene is created by first measuring a small amount of parylene, depending on the final desired thickness, onto an aluminum deposition boat and placed in a deposition chamber. The pressure of the chamber is adjusted with a vacuum to approximately 25 mTorr. A mechanical chiller is used to prevent the parylene particles from leaving the chamber and the furnace is set to 140°C to avoid any parylene deposition on the vacuum gauge.

Once the furnace is heated to 690°C, the parylene melts, which allows it to be poured onto the substrates as it becomes a monomer gas. The parylene is deposited onto the silicon

wafer at room temperature. Once the furnace has chilled, the vacuum is released to unload the silicon wafers from the chamber. The parylene is now peeled from the wafers to be used as a template for preparing microtopography substrates.

To tune the elastic modulus of the substrate for a cardiomyocyte microenvironment, PDMS can be used. PDMS is prepared by mixing a set ratio of elastomer base to curing agent. Details of the preparation are described in the following chapter.

This photolithography process provides a general overview of the bioengineering techniques used to investigate micromechanics of cardiomyocytes. It provides a method of studying cardiomyocyte subdomain contractility and sarcomere assembly when exposed to external cues, and serves as a basis for examining topography effects on stem cells. Micro- and nano- patterned substrates are known to be the most commonly used biomaterials to study physical cue effects on stem cell fate (Reilly, 2010). These substrates provide a non- invasive platform to study mechanotransduction. The external cues that they provide, such as surface topography, composition, and shear stress, have an effect on migration, proliferation, and differentiation of stem cells.

C. Stem Cells in Research

i. Human-Induced Pluripotent Stem Cells

Stem cells are defined by their property of “self-renewal”, the ability to produce more stem cells, and by their ability to make cells that differentiate. In order to achieve these two tasks, stem cells undergo symmetric or asymmetric division (Morrison 2006). In symmetric division, two identical daughter cells with stem cell properties are produced. Asymmetric division gives rise to only one stem cell and a progenitor cell with a limited potential for self-

renewal (Cheng 2008). Stem cells are also classified according to their potency. The categories into which they can fall are: pluripotent, multipotent, or unipotent. Pluripotent cells are able to give rise to any cell type in the body. Stem cells that are multipotent have the potential to give rise to many cells. Their offspring become progenitor cells of cell lines such as blood cells, nerve cells, and skin cells. Adult stem cells are a type of multipotent cell that are used to replace dead or non-functional cells, and are found throughout the body. Unipotent stem cells are specialized to make only one lineage, or cell type, such as skin cells, or cardiomyocytes.

Induced pluripotent stem cells (iPSCs) are a type of pluripotent stem cell that are derived directly from adult stem cells. This technology was developed in 2006 by introducing genes that encode specific transcription factors that could reprogram mature cells into a pluripotent state (Yamanaka 2006). Because of their ability to differentiate into every other cell type, pluripotent stem cells hold great promise for regenerative medicine. iPSCs are used for not only this quality, but also for the fact they do not involve the destruction or manipulation of an embryo. They are derived from adult cells directly, and each individual can have their own stem cell line. In 2007, it was discovered that iPSCs could be created from adult human cells, thus giving them the name human-induced pluripotent stem cells (hiPSCs) (Baker 2007). They are derived by introducing a specific set of reprogramming factors, which are the genes Oct5 (Pou5f1), cMyc, Sox2, and Klf4. Cells then begin to create colonies, which can later be isolated. The derivation process typically is 3-4 weeks. The use of hiPSCs to examine mutations in various cell types, particularly cardiomyocytes, has been a useful tool.

ii. *Human Cardiomyopathy from Genetic Mutation*

Familial point mutations can occur in any protein of the cardiomyocyte and may cause disease, for example, in severe, early-onset myopathy. A mutation can result in a hypertrophic cardiomyopathy (HCM) or a dilated cardiomyopathy (DCM) (Tardiff 2011). In DCM, the heart is enlarged and weakened, the left ventricle wall is thinned, which changes the shape of the chamber to a more spherical one. It is also characterized by systolic dysfunction and a lower ejection fraction. Ventricular remodeling post MI is the main cause of DCM, and familial DCM accounts for nearly half of DCM cases. One particular mutation occurs in cardiac troponin T (cTnT) (Gomes 2004). As a result, force transmission and generation are altered within the sarcomere.

In many cases, DCM occurs as a primary event (Mogensen 2004). Previous studies with cTnT DCM-linked mutations showed that a primary decrease in the calcium sensitivity affected the heart's ability to generate force (Morimoto 2002; Lu 2003). The cTnT region located C-terminal and N-terminal regions is still yet to be functionally and structurally understood (Tardiff 2011).

In one particular familial DCM point mutation, cTnT R173W, family members experience varying levels of DCM. The most severe case occurred in a boy, who needed a heart transplant by the age of 14 (Sun 2012). The point mutation R173W resides in exon 12 of the cardiac Troponin T gene. The TnT2 domain of the C-terminal is bound directly to cTnI and consists of a significant segment of the rigid IT arm between residues 203 to 271 (Tardiff 2011).

There are many TnT2 mutations associated with DCM (Hershburger 2009; Kamisago 2009; Siedman 2011). Because the function of cTnT is to direct the position of tropomyosin between the three known states of myofilament activation, myopathies occur frequently with

TnT2 mutations (McKillop 1993; Pirani 2006). The cTnT mutations have a strong influence in modulating thin filament function and myofilament activation (Tardiff 2011). Calcium binding to cTnC in the troponin complex results in the thick and thin filament interaction, leading to force generation (Kobayashi 2005). DCM models have shown to have a lower sensitivity to calcium in the myofilaments (Pieske 1995; Minamisawa 1999; Rajan 2007), therefore, in order to improve the function of DCM patients, a therapy is required can bring the calcium sensitivity back to the normal physiological range. Treating heart failure by direct modification of sarcomere calcium sensitivity by calcium activators has been previously studied (Solaro 1982; Kass 2006).

A newly designed drug, Omecamtiv Mecarbil, or CK-1827452, was developed as a treatment to increase calcium sensitivity in acute heart failure (Malik 2011). Omecamtiv Mecarbil increases ATP turnover rate by selectively activating the S1 domain of cardiac myosin (Malik 2011). Omecamtiv Mecarbil is energetically neutral and does not lose energy in the power-stroke cycle.

Various symptoms of DCM were found with the cTnT R173W point mutation in the clinic (Sun 2012). To further investigate DCM for a potential treatment, patient-specific hiPSCs were created from skin biopsies from family members that carried the cTnT R173 mutation or not and were reprogrammed into individual iPSC lines (Sun 2012). For the purpose of this study, normal and point mutation single cell iPSC-CMs were examined for functional characteristics at early and late development. Treating these cells with continuous dosing of Omecamtiv Mecarbil could potentially rescue the mutation iPSC-CMs during early development stage, and be used as a therapeutic treatment.

Together, micromechanics of cellular function and bioengineering techniques for regenerative therapy provide an analytical approach to studying cardiac tissue. Findings demonstrate that it is a combination of external and internal cues that influences the function of cardiac cells.

II. Subcellular Contractility and Actin Assembly as Influenced by 3D Microtopography in Neonatal Rat Ventricular Myocytes

A. Overview

In cardiac disease, variations in contractility and sarcomere assembly in cardiomyocytes occur in response to increased external load. These changes occur at the subcellular level to maintain the internal balance of forces along the length and width of the cell. The study here presents the use of microtopography substrates fabricated from stiffness-tunable elastic material to demonstrate how remodeling affects contractility and assembly at the subdomain level of cardiomyocytes. These experiments lead to a better understanding of the structure and function of heart muscle.

B. Materials and Methods:

i. Fabrication of BioMEMS Substrates

The process of fabricating microtopography substrate surfaces has previously been described by our lab (Motlagh et al. 2003). In brief, a UV photolithography process was conducted using SU-8 photoresist (MicroChem, Newton, MA) on silicon wafers. Using a chemical vapor process, the wafer with topography surface is made into a parylene template. The parylene was removed from the wafer to be used as a secondary template for molding topography surfaces on polydimethylsiloxane (PDMS) (Dow Corning, Midland, MI). For a 100 kPa substrate, a 50:1 elastomer base to curing agent ratio was used to create PDMS, and was rapidly mixed for approximately five minutes. The bulk PDMS was placed in a vacuum desiccator for approximately thirty minutes to remove any air bubbles. The PDMS was then spun onto cell culture-compatible plates (MatTek, Ashland, MA) to create a thickness of approximately 30 microns. To create microtopography substrates, the parylene was placed on

PDMS and degassed again for approximately ten minutes. To cure the PDMS substrates, the dishes were placed in a 60°C oven for 24 hours. The PDMS was then cooled and the parylene template was removed, which left the PDMS substrates with a microtopography surface. The resulting substrate has a stiffness of 100 kPa and cylindrical microposts that are 15 µm high and spaced 75 µm apart, in a tetragonal array.

ii. Substrate Stiffness

To test the PDMS substrate stiffness, Atomic Force Microscopy (AFM) techniques were used. First, a Borosilicate Glass Particle (10 µm) on Silicon Nitride (0.12 N/m) cantilever tip was calibrated with respect to a glass surface. Six measurements were conducted in a region of cured PDMS, cantilever was moved to a different region, and six new measurements were taken. This process was repeated approximately three times per substrate. The stress-strain properties of the material as related by Young's Modulus of elasticity were tested in on a minimum of three samples, each from a different mixing batch of PDMS, resulting in a total of 53 sample points measured for the mixture.

2.3 Substrate Preparation for Cell Culture

A solution of 5% APTES (3-aminopropyltrimethoxysilane) in a 5% water, 200 proof isopropyl alcohol mixture was prepared and poured on the substrates for 10 minutes. This mixture was then aspirated, and the substrates were washed with 200 proof isopropyl alcohol. The substrates were placed in the oven at 60° C for 25 minutes and cooled for 5 minutes before washing the substrates with a mixture of 5% water and 200 proof isopropyl alcohol. The substrates were then coated with a fibronectin (20 µg/ml) in DMEM solution and placed in an incubator (37°C and 5% CO₂) for 2 hours prior to seeding cells.

iv. NRVM Culture

Primary cardiomyocyte cultures were obtained from neonatal rat ventricular myocytes (NRVM) in accordance to NIH and Institutional Animal Care use guidelines for the care and use of laboratory animals. Hearts from 1-2 days old neonatal Sprague-Dawley rats with collagenase (Worthington) were removed and cells were isolated as previously described by our lab (Boateng et al. 2003; Curtis et al. 2012). The cells were resuspended and filtered through a metal sieve to remove large materials, so that they could be plated at a low density (250,000 cells/dish) in PC-1 medium (Biowhittaker /Cambrex) on the substrate surfaces coated in fibronectin. The dishes were then placed in a 37° C, 5% CO₂ incubator, and left undisturbed for 24 hours. PC-1 media was replenished every two days, and unattached cells were removed by aspiration.

v. Immunohistochemistry

NRVMs were fixed in 10% paraformaldehyde for 10 minutes, and then a 0.3 M glycine/PBS (Media Tech, Manassas, VA) rinse. NRVMs were next incubated in 0.5 % Triton X-100 (Sigma St. Louis, MO) for 10 min in order to permeabilize NRVM membranes. NRVMs were labeled with a primary antibody for sarcomeric α -actin to label the Z-disk (mouse monoclonal ab9465, Abcam, Cambridge, MA) diluted 1/200 and paxillin to label the focal adhesion (rabbit monoclonal ab9465, Abcam, Cambridge, MA) diluted 1/250 in 1 % TBST (Sigma St. Louis, MO), /1 % BSA (Sigma St. Louis, MO) /PBS and left overnight in a 4° F refrigerator. NRVMs were then washed multiple times with PBS and incubated with goat anti-mouse Alexa Fluor IgG 488 and mouse anti-rabbit Alexa Fluor IgG 568 secondary antibody (Invitrogen) diluted at a 1/1000 ratio for 45 min in room temperature. All samples were washed with PBS then preserved in 1 nM 4',6-diamidino-2-phenylindole (DAPI)/PBS (Vector Labs, Burlingame, CA) to label nuclei. Dishes were stored in a 4°F refrigerator until imaged.

vi. *Fluorescence Confocal Microscopy*

NRVM images were captured via a Zeiss LSM Observer Z1 microscope (Zeiss, Peabody, MA) to create 1024×1024 pixel images using a 63x objective lens for assessment of NRVM surface area using ImageJ. Z-stacks were collected with 1024×1024 pixel resolution and $0.5 \mu\text{m}$ optical slices using a Zeiss 710 Confocal Microscope (Zeiss, Peabody, MA) with a 40x or 63x objective lens with laser wavelengths of either 488 or 568 nm.

vii. *Measuring Shortening and Shortening Velocity*

Line scans as a method to gain detailed information about myofibrillar contractility has been previously reported by our lab (Curtis 2012; Broughton 2014). Beating cardiomyocytes were examined under a Zeiss 710 Confocal Microscope (Zeiss, Peabody, MA) with a 25x objective (Zeiss). Cells that were selected for analysis were isolated (single cell), possessed a major axis visually longer than the minor axis, and attached to a post.

A line scan was taken along the longest axis of the cell by using Zen software (Zeiss), which correlated to the myofibril with the greatest shortening (Figure 5). A differential interference contrast channel transmitted light from which a line every 30 ms over the course of 1000 ms, thus recording multiple complete and regular cycles of NRVM contraction. From the motion generated by the NRVM, peaks of contraction were used as an indicator of shortening and shortening velocity, and were used to mark regions of maximum shortening and the relation of distance to time, as described by our lab previously (Curtis 2012; Broughton 2014). Image processing software (LSM Browser, Zeiss) was used to obtain the shortening and velocity in a single cell contraction by scaling the pixel to micron distance as well as the time.

Measurements were taken two days after plating cells on PDMS micropost substrates. Measurements comparing NRVMs plated on flat substrates were also taken at two days after plating. The maximum shortening and velocity for NRVMs with a major myofibrillar axis were measured at 3 different regions: the region closest to the post, the region in the middle of the NRVM, and the region furthest away from the post, towards the end of the cell. Cell length was also measured. Measurements were made in a total of at least forty NRVMs over the course of three separate experiments per condition.

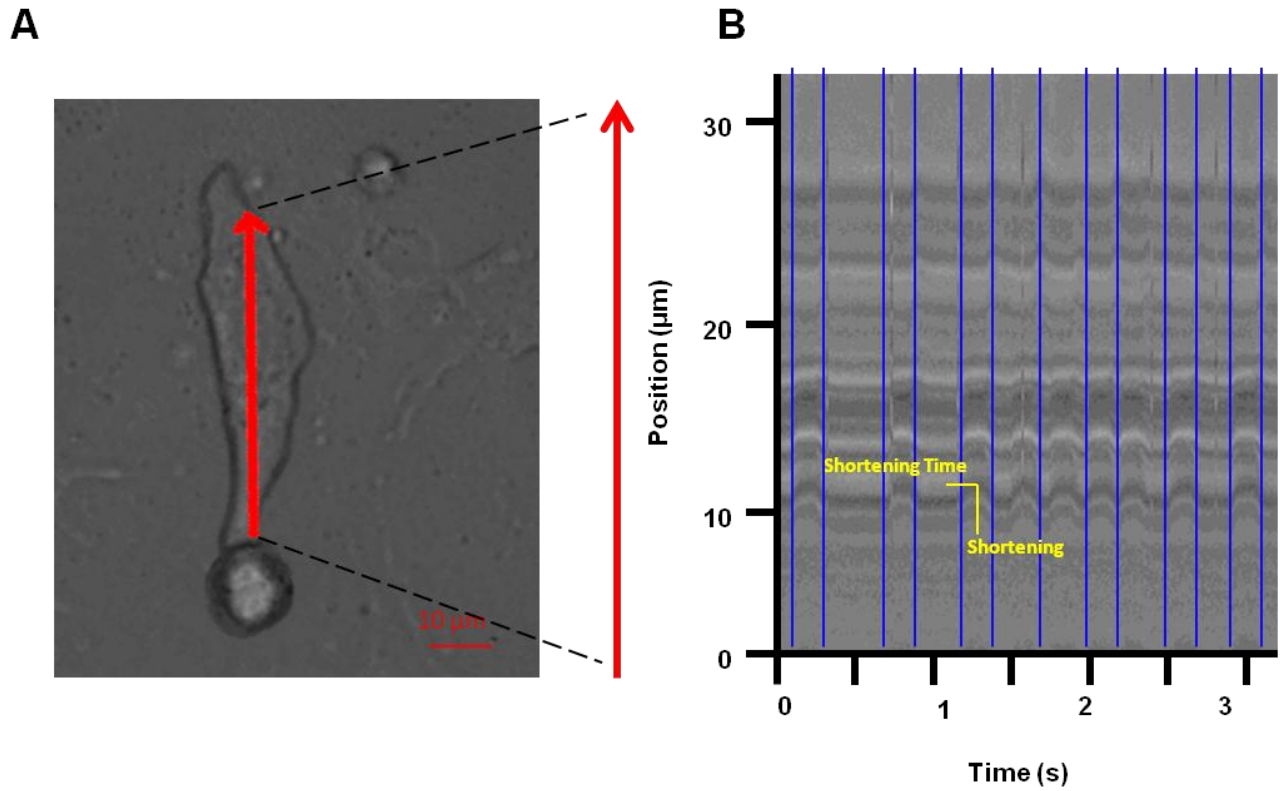


Figure 5: Measurement of Neonatal Rat Ventricular Myocyte Shortening, Shortening Velocity, and Beat Frequency using a Kymograph. (a) Contractility was recorded in a single NRVM anchored to a 100 kPa Post, via a line scan (red line). (b) Kymograph of cell displacements (red arrow line scanned over time) shows maximum displacement, at which the shortening time is recorded. Blue lines show the start and end of a contraction that are used to calculate the beat frequency.

viii. *Actin FRAP Dynamics*

To examine sarcomere assembly in each region of the cell, analyses of fluorescence recovery after photobleaching (FRAP) experiments were conducted. Forty-eight hours after cell isolation, actin-GFP expression was induced by Cell-Light Reagents BacMam 2.0 actin-GFP. Two days after NRVM isolation, appropriate volume of CellLight Reagent (30 µl/500,000 cells) was used as modified from the manufacturer's instructions. Infected NRVMs are returned to the culture incubator for at least 16 h.

ix. *Analysis of fluorescence recovery after photobleaching*

FRAP analysis was conducted as previously described by our lab (Lin et al. 2013). Up to 10 beating and well-striated cells (as evidenced by actin-GFP) were randomly selected for each FRAP. FRAP images were obtained by a Zeiss LSM 710 confocal microscope. The intensity (I_{FRAP}) of the region of interest (ROI; area = 3.75 µm x 3.75 µm) was observed both before (t_0) and after (t_1) bleaching at full power. Data were collected every 10 seconds, because of the high dynamics of actin, for a total duration of 8 minutes. FRAP analysis was conducted and measured three times for 3 different regions: the region closest to the post, the region in the middle of the NRVM, and the region furthest away from the post, towards the end of the cell. Images were analyzed using the Zeiss Imaging Browser. Plotted intensity values were given as a percentage of the difference between $I_{\text{FRAP}}(t_0)$ and $I_{\text{FRAP}}(t_1)$. Because actin binding has one binding state, the equation for curve fitting using nonlinear regression in OriginPro was:

$$I_{\text{frap}}(t) = 1 - C_1 e^{-K_{\text{off1}} t}$$

The average kinetic constant (K_{frap}) was calculated using the following formula:

$$K_{\text{frap}} = C_1 K_{\text{off1}}$$

x. Statistical Analysis

Data was recorded and sorted using Excel software (Microsoft, Redmond, CA) and statistical analysis was conducted using GraphPad Prism (GraphPad Software, La Jolla, CA). Significant differences in variables were calculated by using either two-tailed Student's t-test or n-way ANOVA. Statistics were based on a minimum sample size of 10 NRVMs per condition total from a minimum of four experiments per sample set. All NRVM data were expressed as mean \pm one standard error of the mean. For FRAP assays, the sample number was defined as individual cells, of which one to five cells were analyzed per culture in at least three separate cultures analyzed per experimental condition.

C. Results

i. *Substrate Stiffness*

Using the polymerization time and temperature described in the previous section, it was found that a 50:1 ratio to results in a Young's Modulus of 98.4 ± 7.34 kPa. The 100 kPa (50:1 ratio) was the softest PDMS substrate that could be used to form microposts which can retain their shape once the parylene is removed to mimic normal heart tissue stiffness (Berry 2006; Bhana 2010; Borbely.2005; Omens 1998).

ii. *Cell Structure Influence from Microposts*

Real-time imaging of cardiomyocytes was used to observe the behavior of cells in relation to the microtopography as compared to the adherence on a flat substrate after cell plating. Over time, it was observed that cardiomyocytes remodel closer with respect to the microposts, demonstrating that it was probable that the nucleus also remodels against the micropost. It was additionally observed that cells on flat substrates did not remodel myofibrils in a similar manner nor was the nucleus likely to reposition.

iii. *Shortening and Shortening Velocity as a Function of Distance from Micropost*

Cardiomyocyte shortening and shortening velocity was calculated through the use of kymographs, which showed the contractile pattern along the major myofibril axis of the cell (Figure 5). The area with the maximum shortening and velocity were greatest towards the centroid region of the cell (0.65 ± 0.29 μm at 1.78 ± 0.30 $\mu\text{m/s}$), lower in the region near the post (0.94 ± 0.11 μm at 2.82 ± 0.17 $\mu\text{m/s}$), and lowest in the region furthest from the post (0.52 ± 0.26 μm at 1.03 ± 0.34 $\mu\text{m/s}$) (n=45 cells, 3 measurements per cell) (Figures 6 and 7). The average shortening and shortening velocity on the flat substrate was 0.57 ± 0.12 μm at

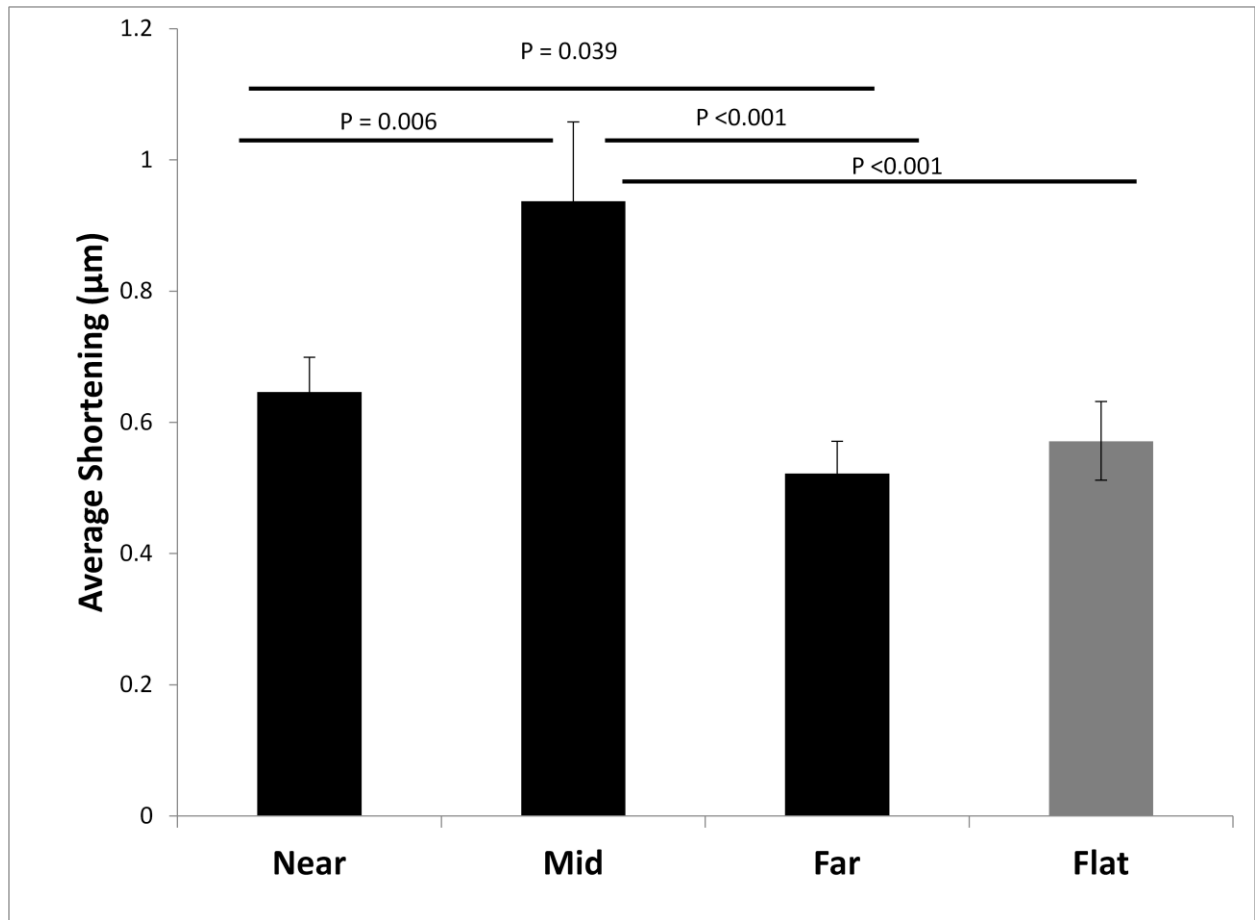


Figure 6: NRVM Shortening Varies as a Function of the Distance from the 3D Micropost. Maximum shortening was found in the middle region of NRVMs (100 kPa PDMS), as compared to the region near and far from the post and flat 100 kPa substrata. n=45 cells with 3 contraction samples per cell.

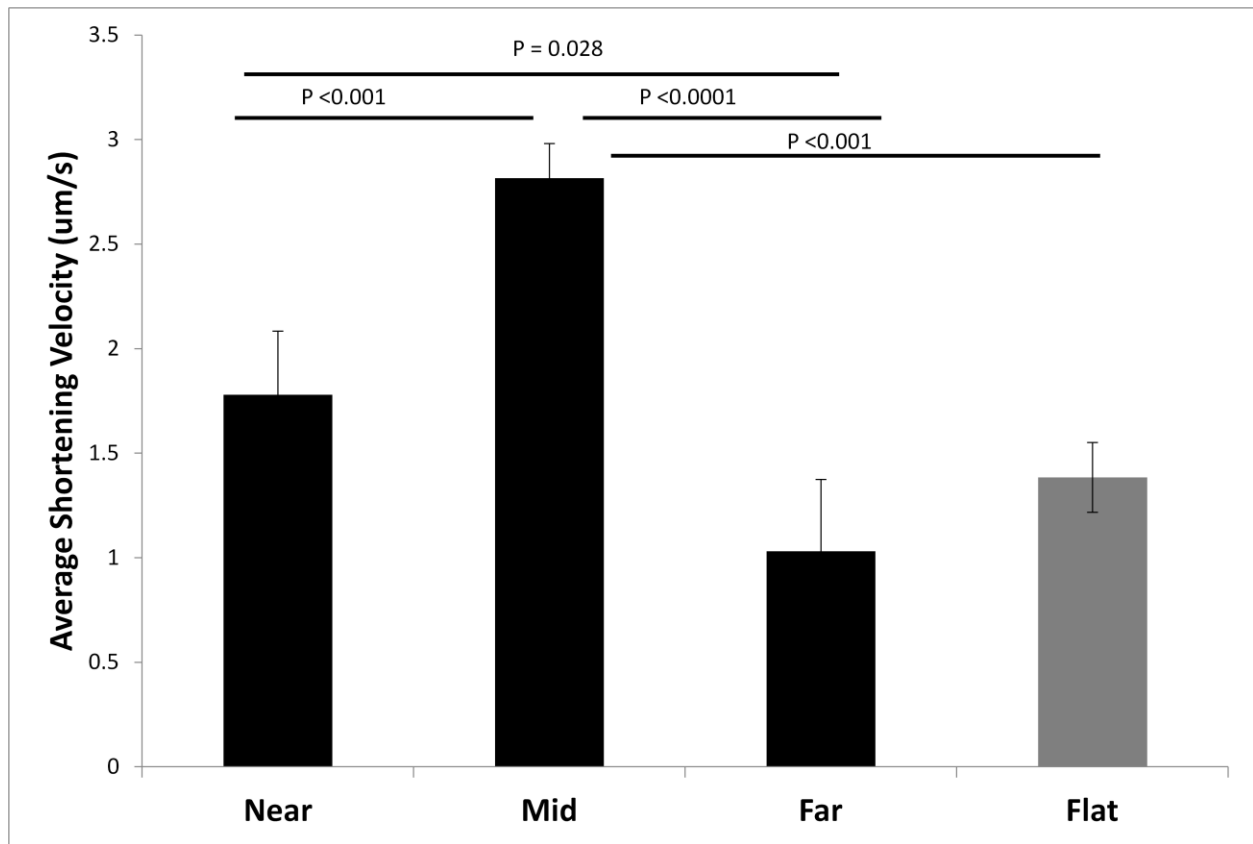


Figure 7: NRVM Shortening Velocity Varies as a Function of Distance from the 3D Micropost. Maximum shortening velocity was found in the middle region of NRVMs on posts (100 kPa PDMS), as compared to the region near and far from the post and flat substrata (100 kPa). n=45 cells with 3 contraction samples per cell.

$1.38 \pm 0.17 \mu\text{m/s}$. The variation in shortening and shortening velocity in the different regions of the cell demonstrated that its mechanics were regulated locally within a cell. The mid-post region shortening was significantly higher than the near-post region ($p = 0.006$), far-post region ($p < 0.001$), or the flat substrate ($p < 0.001$). The near-post region was significantly higher than the far post region ($p < 0.001$) ($n=45$ cells) (Figures 6 and 7).

iv. *Actin FRAP Dynamics as a Function of Distance from Micropost*

To study the effect of static load provided by 3D micropost on actin filament assembly, the dynamics of sarcomeric actin were measured through FRAP in NRVMs. The cells were infected with actin-GFP fusion virus to visualize the striated pattern and quantify the recovery profile of the actin-GFP fluorescence (Figure 8). The kinetic constant (K_{FRAP}) obtained from the results of the curve fitting was significantly greater in the cell region near to the post ($6.5 \times 10^{-4} \text{ sec}^{-1} \pm 1.4 \times 10^{-4}$) as compared to a cell on a flat substrata ($2.5 \times 10^{-4} \text{ sec}^{-1} \pm 6.5 \times 10^{-5}$) ($p < 0.0001$) ($n=14$) (Figure 9). The kinetic constant (K_{FRAP}) near the post was also significantly higher than the mid-region of the cell ($3.9 \times 10^{-4} \text{ sec}^{-1} \pm 1.4 \times 10^{-4}$) ($p = 0.04$) ($n=14$), and the region furthest from the cell ($1.9 \times 10^{-4} \text{ sec}^{-1} \pm 7.8 \times 10^{-5}$) ($p = 0.048$) ($n=14$) (Figure 10). The actin FRAP dynamics were not significantly different in the cells on flat surfaces (100 kPa) as compared to the “far” region of the cell anchored to a micropost.

v. *PKC- ϵ concentration near Micropost*

A further understanding of the localized variability within a cell was carried out through quantifying the concentration of the PKC-epsilon enzyme throughout a cardiomyocyte, which is known to enhance cardiac contractility and remodeling. The area of the NRVM anchored along the micropost exhibited a higher fraction of PKC-epsilon (0.427), than the middle and far regions (0.296 and 0.277) (Figure 11). Percent fluorescence was calculated by ImageJ software.

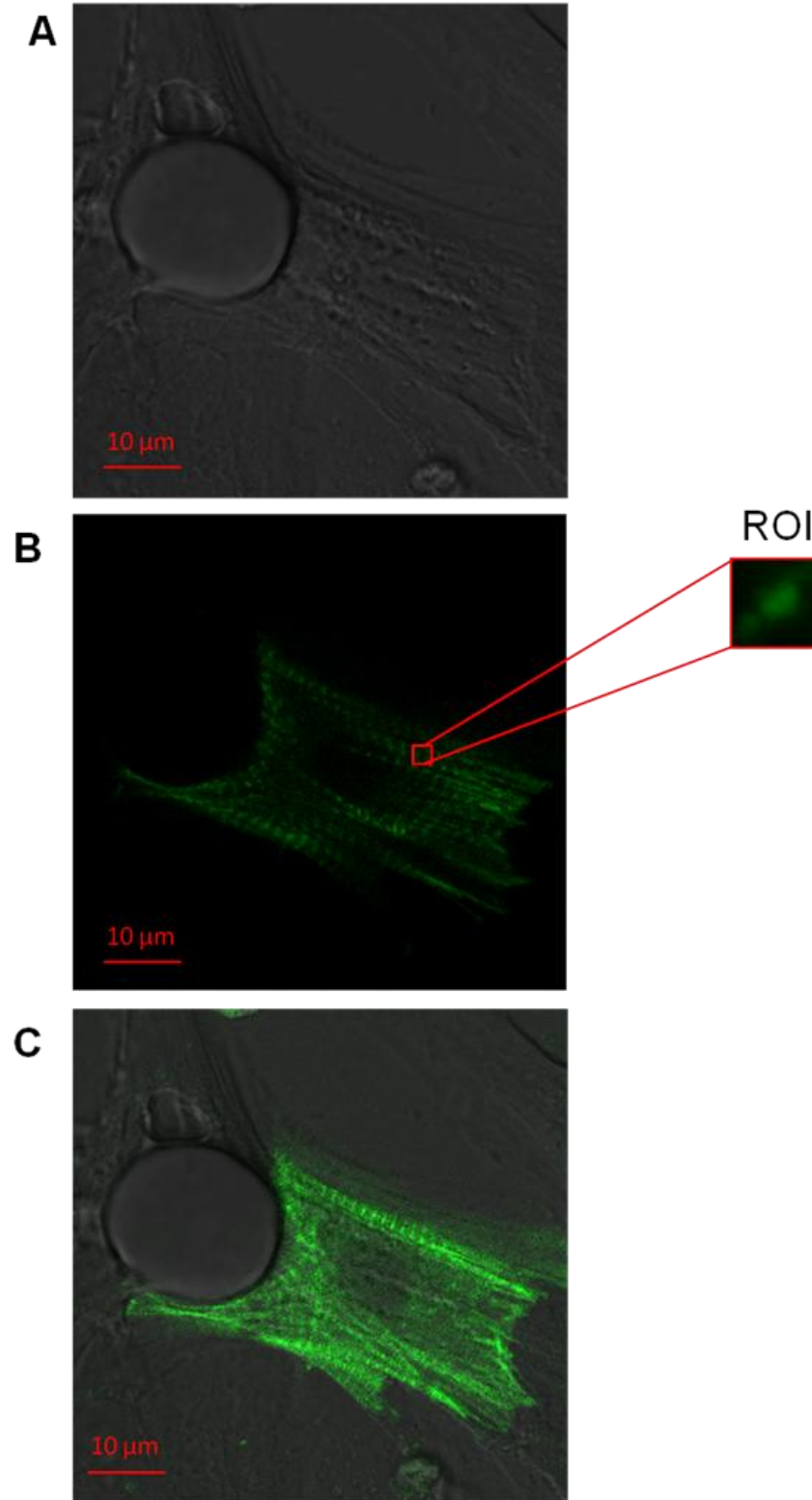


Figure 8: Actin-GFP Dynamics in NRVM. Confocal images: (A) Phase contrast, (B) Fluorescent, (C) Merged show the localization of actin throughout the cell. Red box denotes Region of Interest (ROI) of a striation in which FRAP was analyzed.

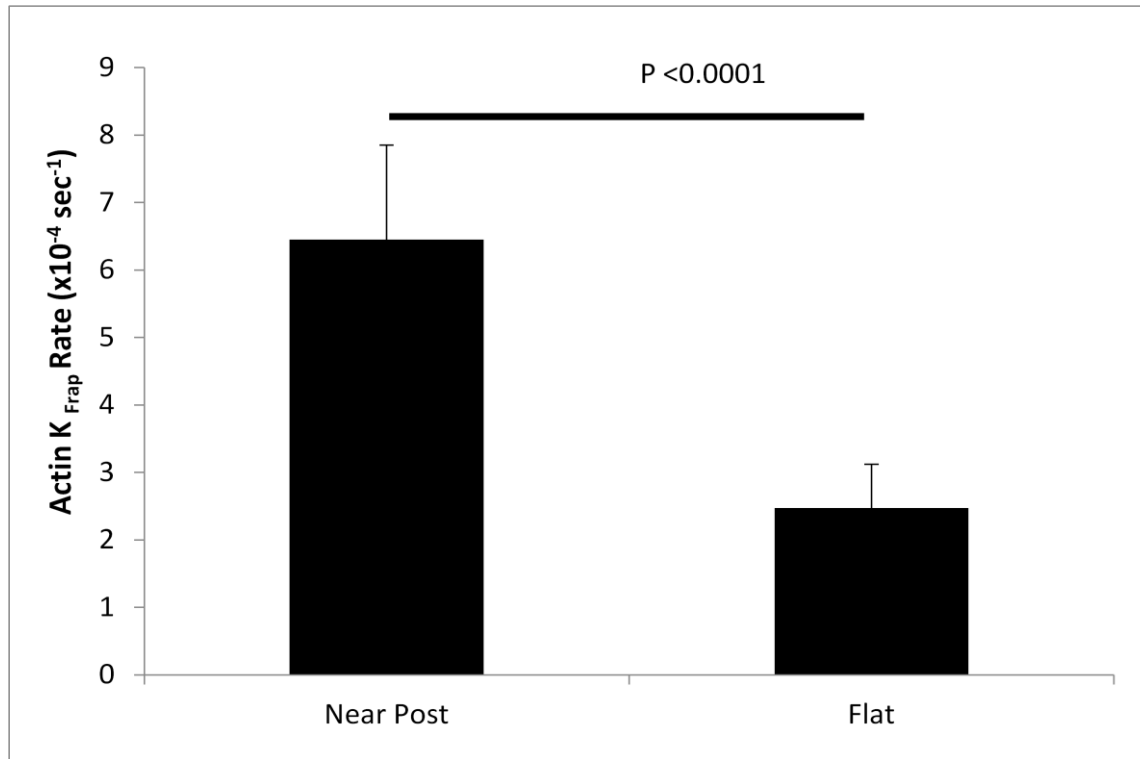


Figure 9: Actin Dynamics with 3D attachment. 3D cell anchorage near micro post increases actin K_{FRAP} rate as compared to flat substrata (100 kPa) $n = 14$ cells

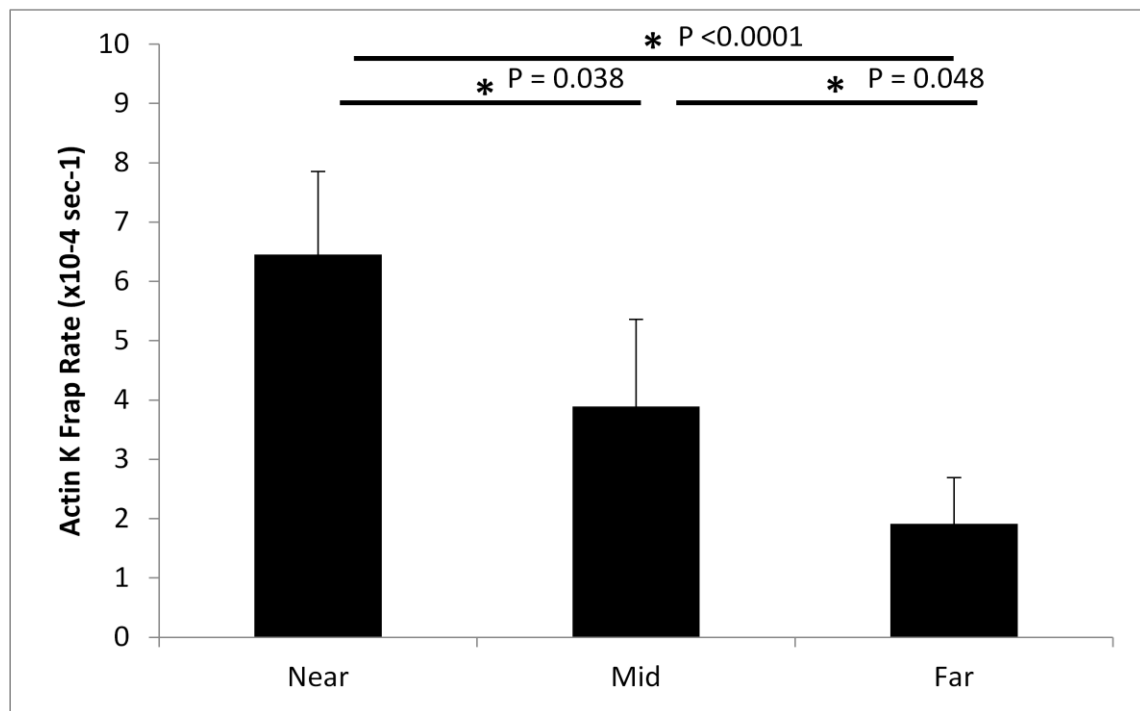


Figure 10: Actin Dynamics as a Function of Distance from Micropost Actin FRAP rate at positions near, middle, or far from the 3D cell anchorage on the micropost at 100 kPa. Actin FRAP dynamics dominates adjacent to the micropost (n=14).

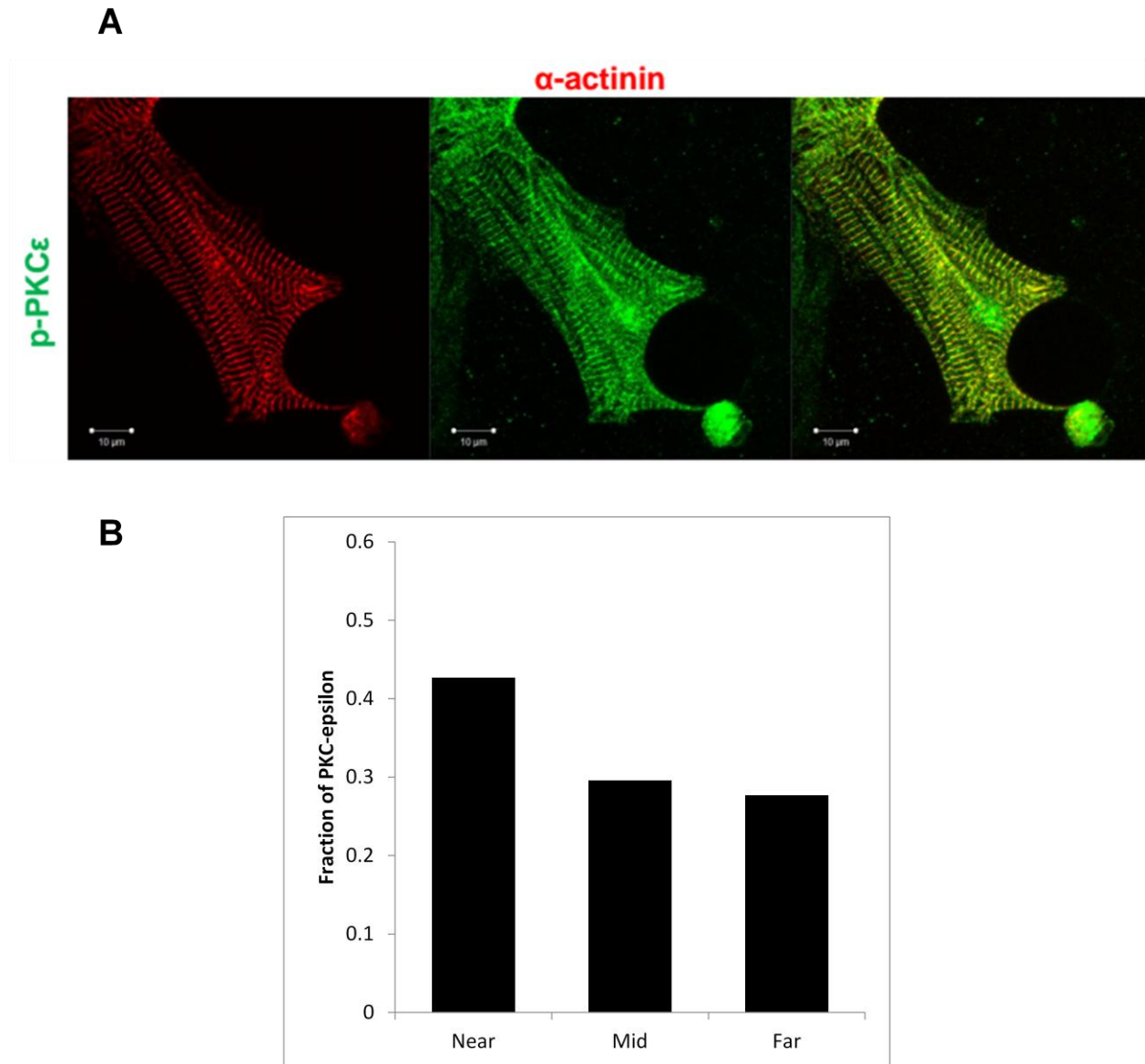


Figure 11: PKC- ϵ Distribution as a Function of Distance from the 3D Micropost

(A) Confocal images of NRVM attached to a micropost demonstrating PKC epsilon distribution. (B) Fraction of PKC-epsilon adjacent to post, n= 1 cell. In collaboration with Jieli Li, MD, PhD.

D. Discussion

An important finding from this study was that cardiomyocyte contractility and actin assembly are both subdomain regulated. It was evident that variations existed in the shortening and the shortening velocity in each individual sarcomere within the myofibril and each region of the cell attached to a post. The data collected from the line scan and actin FRAP experiments suggested that mechanical load and shortening both contributed to actin assembly. Within a cardiomyocyte, each individual concentric contraction is generated by the interaction of actin and myosin - otherwise known as the length-tension relationship (Huxley 1969). A decrease in shortening velocity correlated with an increase in stress, and surface tension occurred. Additionally, cells plated on a 3D surface, compared to a flat surface had an increased external load, indicating they had better contractile properties. It has been previously noted that regions of the cell with decreased shortening velocity correlated with regions of higher force, as measured with traction force microscopy (Hazeltine 2012; Broughton 2014).

The microposts provided a significant amount of load onto the anchoring edge of cardiomyocytes as demonstrated by the varying shortening velocities. As discussed before, the cells arrange themselves such that the bulk of their mass is located near the post along with the nucleus, and the least mass furthest away from the post. The observed velocities and forces can be explained with regards to the force-velocity relationship. The force generated by the muscle is dependent on the number of total cross bridges attached (Sayers 2005). Force decreases when there are fewer cross bridges attached, since it takes a finite length of time for their attachment, as filaments slide past each other with increasing velocity. On the other hand, as the relative muscle filament velocity decreases, there is more time for cross bridges to attach and generate

force, and therefore force increases. The results demonstrated that rate constants of cross-bridge attachment affect force generation.

Muscles grow when additional force is applied. Where there are greater forces, there is more muscle growth. Therefore, when exercises are performed in which muscle contractions occur at high velocities, they are also contracting at relatively low force. This phenomenon is intuitive when considering lifting a light load compared to a heavy load - the light load is easy to move. However, because the muscle forces would be lower, these movements would have a very little affect on hypertrophy.

Similar effects of cardiomyocyte force generation on a micropost were observed in various other studies. A study that examined the deflection of microposts in response to myocyte anchorage showed that measured traction forces were greatest on either ends of the myocyte attached to PDMS posts (Cheng 2013). The traction forces near the center of the cell were relatively small (Cheng 2013). Muscle cells attached on top of a field of microposts shows the highest tension near the bending posts, and a linear relationship between the applied force and the post displacement (Sniadecki 2007; Norman 2008). Interestingly, coating substrates with different ECM proteins also regulates the contractility of cardiomyocytes, as higher surface binding strength and stability were observed in laminin and APTES-coated microtopography substrates (Ribiero 2014).

The dynamics of sarcomeric actin, which is a main regulator of actin-filament assembly, was found to be elevated in the cell region closest to a post, where there was the greatest mechanical load. It is known that increased load alters actin assembly during hypertrophy. These results are consistent with the effect of mechanical strain on dynamics, which demonstrated that an hour of cyclic strain on a cell was sufficient to increase the dynamics of sarcomeric actin,

compared to a cell that was not exposed to any strain (Lin et al. 2013). FRAP experiments demonstrate a vital role of the binding affinity between constituents in the Z-disk involved in sarcomere formation. It is perceived that certain signaling molecules, weaken Cap-Z binding to actin by loosening the Z-disk, thus opening new opportunities for new filament assembly (Russell 2010). PKC ϵ has shown to induce changes in myocyte cell shape, leading to an increase in the overall cell length (Strait 2001; Heidkamp 2003). Findings showed that there was a higher PKC ϵ fluorescence fraction near the post, indicating an increased need for PKC ϵ activation for remodeling the sarcomere. This area adjacent to the microstructure has larger focal adhesions, or more paxillin, and a thicker layer of filaments with well-organized sarcomeres (Broughton 2014) - which was evident in the increased protein dynamic exchange.

This study shows that the cardiomyocyte region with the greatest shortening and velocity was towards the middle region of the cell, whereas the greatest actin dynamics occurred in the near-post region. With the 3D microtopography, the cell remodels itself with the most mass anchored against a post, and the least mass furthest away from the post. Therefore, there is a constant balance of forces that occurs within the cell in order to maintain effective function. A conclusion can be made that sarcomere assembly is largely impacted by mechanical load distribution throughout the cell. Further studies can be carried out to better understand the relationship between force distribution and sarcomere assembly.

E. Conclusion

The novel use of 3-dimensional topography soft substrates to mimic the life-like environment of a cardiomyocyte serves as an excellent tool to study mechanics of the cell. This is critical to understand the cell's behavior to respond to physical and biochemical cues of its environment. When grown on posts, cardiomyocytes show increased contractility patterns and actin dynamic exchange.

When examining these characteristics at the subdomain level, it is clear that differences in physical cues throughout the cell correlate with the cell's response. The subdomain regulation of cell function is related to the surrounding environment and measured by line scans or FRAP experiments. The techniques used in this study for measuring subcellular forces can be used in the future in clinical research involving human diseases with cardiomyocytes.

III. Sarcomere Structure and Assembly in Normal Human and cTnT Mutation Cardiomyocytes Derived from Induced Pluripotent Stem Cells

A. Overview

Sarcomeric familial point mutations that occur in cardiac troponin T (cTnT) have been shown to cause early-onset myopathy (Sun 2012). Dilated cardiomyopathy (DCM) can result from a sarcomeric point mutation, such as cTnT R173W. For this study, cardiomyocytes derived from induced pluripotent stem cells (iPSC-CMs) from affected patients that carried the cTnT R173W mutation and serve as a platform for examining their functional characteristics during early and late development, as compared to iPSC-CMs from normal family members. The cells were also treated with 200 nM dose Omecamtiv Mecarbil to test whether this drug could therapeutically rescue the mutation cells during its development stage. This study demonstrates the differences between the structure and function of normal and cTnT R173 point-mutation iPSC-CMs.

B. Materials and Methods

i. Substrate Fabrication

The process of fabricating flat PDMS substrates has previously been described by our lab (Motlagh et al. 2003). For a 100 kPa substrate, a 50:1 elastomer base to curing agent ratio was used to create PDMS, and was rapidly mixed for approximately five minutes. The PDMS was placed in a vacuum desiccator for approximately thirty minutes to remove any air bubbles. The PDMS was then spun onto cell culture-compatible plates (MatTek, Ashland, MA) to create a thickness of approximately 30 microns. To polymerize the PDMS substrates, the dishes were placed in a 60°C oven for 24 hours. The PDMS was then cooled and ready for cell-plating

preparation. The PDMS stiffness was measured using AFM and found to be 100 kPa, as previously described.

ii. Substrate Preparation for Cell Plating

Substrates were first washed with 200 proof isopropyl, then washed three times with PBS. The substrates were then layered with a coat of a 1:60 solution of Matrigel Basement Membrane Matrix Growth Factor Reduced (BD Biosciences, San Diego, CA) / DMEM/ F12 1:1 (Life Technologies, Grand Rapids, NY) and kept in an incubator (37° C at 5% CO₂) incubator for 30 minutes before seeding the cells.

iii. iPSC-CM Culture

The procedure of converting iPSCs into the cardiac-specific lineage (iPSC-CMs) is well documented (Sun 2012; Burrige 2014). In short, fibroblasts taken from skin biopsies of patients who either were or were not afflicted with the cTnT R173W mutation from the same family were reprogrammed with lentiviral Yamanaka 4 factors (Oct4, Sox2, Klf4 and c-MYC) under feeder-free conditions (Sun 2012). Colonies with human stem cell (hESC)-like morphology were chosen, expanded, and recognized as individual iPSC lines. All iPSC lines were confirmed to either have or not have the cTnT R173W mutation in addition to expressing the pluripotency markers TRA-1-81, Oct 4, Nanog, and SSEA-4. iPSC lines that had an incomplete transgene silencing were removed from the following studies (Sun 2012).

The iPSCs were then transformed into the cardiovascular lineage (iPSC-CMs) using a well-documented 3D differentiation protocol (Yang 2008). For these studies, the iPSC-CMs went through 19 passages before they became completely derived into a cardiovascular lineage. The iPSC-CMs were then distinguished by their spontaneous beating and electrophysiological

properties (Sun 2008). Finally, iPSC-CMs were aliquoted into 1-2 million cells per 1 mL media, frozen and stored in a -80° C freezer.

iPSC-CMs from one control (unaffected) line and one line affected with the cTnT R173W point mutation were prepared at Stanford University in the laboratory of Dr. Joseph Wu. They were shipped in vials containing 1-2 million cells, and stored in a -80° C freezer until used. When cells were needed for use, thawing and plating procedures previously established were used (Sun 2012). In brief, cell vials were thawed in warm bath water. Cells were then suspended in RPMI (Life Technologies, Grand Rapids, NY) and centrifuged at 500 RPM for 5 minutes into pellets. The supernatant was then removed by aspiration and the cell pellets were re-suspended in RPMI with 2% B-27 supplement with Insulin (Life Technologies, Grand Rapids, NY), 1% Pen-Strep antibiotic (Life Technologies, Grand Rapids, NY) and 2% Fetal Bovine Serum (Life Technologies, Grand Rapids, NY) to improve cell attachment. The matrigel-coated substrates were then taken from the incubator to aspirate the matrigel. The cells were then seeded at low density (250,000 to 500,000 cells/ 35 mm dish) on the substrates and returned to the incubator (37° C, 5% CO₂) until the time for experiments. The media (RPMI with 2% B-27 supplement with Insulin and 1% Pen-Strep) was aspirated and replaced out every 2 days.

iv. Real-time Phase Imaging

iPSC-CMs were examined under a Zeiss LSM Observer Z1 microscope (Zeiss, Peabody, MA) with a 63x objective lens. Videos were recorded with phase microscopy of the randomly-selected cells for fifteen seconds. The beats per minute (BPM) was observed each day for untreated normal and mutation cells from 2-14 days after plating. Detailed studies were conducted at Week 1 (between days 5-8) and Week 2 (Days 12-14).

v. *Immunohistochemistry*

iPSC-CMs were fixed in 10.0 % paraformaldehyde, and next a 0.3 M glycine/PBS (Media Tech, Manassas, VA) rinse. iPSC-CMs were then incubated for 10 min to permeabilize membranes with 0.5 % Triton X-100 (Sigma St. Louis, MO). iPSC-CMs were labeled with a primary antibody for sarcomeric α -actinin (mouse monoclonal ab9465, Abcam, Cambridge, MA) diluted 1/200 and phalloidin (Invitrogen) diluted 1/1000 in 1 % TBST (Sigma St. Louis, MO), 1 % BSA (Sigma St. Louis, MO), PBS and left overnight in a 4° F refrigerator and then washed with PBS. iPSC-CMs were then washed multiple times with PBS and incubated for 45 min in room temperature with rabbit anti-mouse Alexa Fluor IgG 488 antibody (Invitrogen) diluted 1/1,000. For an F-actin stain, the cell membranes were permeabilized, and a phalloidin 568 fluorescence (Invitrogen) was diluted 1/100 in 1% TBST/1% BSA/PBS mix in room temperature for 45 min and then washed with PBS. All cells were kept in 1 nM 4',6-diamidino-2-phenylindole (DAPI)/PBS (Vector Labs, Burlingame, CA), which stains for the nucleus, and stored in a 4°F refrigerator until imaged. iPSC-CM images were collected at 1024 × 1024 pixels using a Zeiss LSM Observer Z1 microscope (Zeiss, Peabody, MA) with a 63x objective lens to analyzed the iPSC-CM myofibril development using fluorescent wavelengths of 358, 488 or 568 nm.

vi. *Measuring Shortening and Shortening Velocity*

Line scans as a technique to gain information about myofibrillar contractility has been previously reported by our lab (Curtis 2012; Broughton 2014). Beating iPSC-CMs examined under a Zeiss 710 Confocal Microscope (Zeiss, Peabody, MA) with a 25x objective (Zeiss).

A line scan was taken along the long axis of the cell by using Zen software (Zeiss) (Figure 12). A differential interference contrast channel transmitted light and was captured from each line every 30 ms over the course of 1000 ms, which recorded several complete and normal cycles of iPSC-CMs contraction. From the motion generated by the iPSC-CMs, peaks of contraction were used as an indicator of shortening velocity, and were used to mark regions of maximum shortening and the relation of distance to time, as described by our lab previously (Curtis 2012; Broughton 2014). Image processing software (LSM Browser, Zeiss) was used to obtain the shortening and velocity in a single cell contraction by scaling the pixel to micron distance as well as the time. These measurements were taken one and two weeks after plating cells on PDMS substrates. The maximum shortening and associated velocity for iPSC-CMs with was measured for ten contractions per iPSC-CMs.

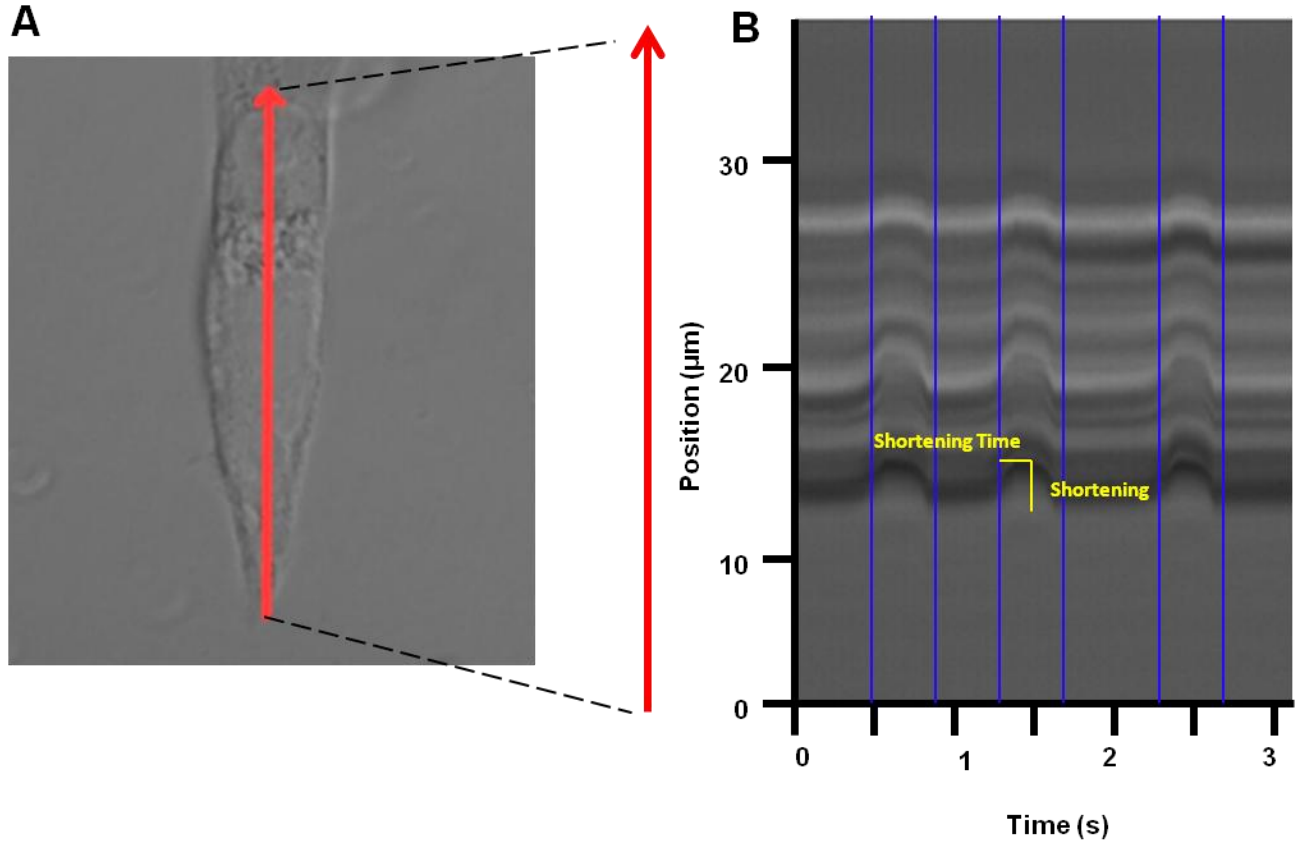


Figure 12: Measuring Shortening, Shortening Velocity, and Beat Frequency in iPSC-CMs using a Kymograph. (a) Contractility motion was measured in a single iPSC-CM, via a line scan (red line). (b) Kymograph of cell displacements over a period of time shows maximum shortening, at which the time of shortening is measured. Blue lines indicate the beginning and end of a contraction and peak-to-peak time used to calculate beats per minute.

vii. *Actin FRAP Dynamics*

To examine sarcomere assembly in iPSC-CMs, analyses of fluorescence recovery after photobleaching (FRAP) experiments were conducted. These experiments were conducted up to 2 weeks after plating the cells. Actin-GFP expression was induced by Cell-Light Reagents BacMam 2.0 actin-GFP in a two-day infection process. Two days before experiments, an appropriate volume of CellLight Reagent (35 µl/500,000 cells) was used as modified from the manufacturer's instructions. One day before experiments, a volume of 70 µl/500,000 cells of CellLight Reagent was used in each of the dishes. Infected iPSC-CMs were returned to the culture incubator for at least 16 hours.

viii. *Analysis of fluorescence recovery after photobleaching*

Fluorescence recovery after photobleaching (FRAP) analysis was conducted as previously described by our lab (Lin et al. 2013). iPSC-CMs that showed a green actin-GFP label, were selected for each FRAP. FRAP images were obtained by a Zeiss LSM 710 confocal microscope. The intensity (I_{FRAP}) of the region of interest (ROI; area = 3.75 µm x 3.75 µm) was observed both before (t_0) and after (t_1) bleaching at full power. Data were collected every 10 seconds, because of the high dynamics of actin, for a duration of 8 minutes. Images were analyzed using the Zeiss Imaging Browser. Plotted intensity values were given as a percentage of the difference between $I_{\text{FRAP}}(t_0)$ and $I_{\text{FRAP}}(t_1)$. Because actin binding has one binding state, the equation for curve fitting using nonlinear regression in OriginPro was:

$$I_{\text{frap}}(t) = 1 - C_1 e^{-K_{\text{off1}} t}$$

The average kinetic constant (K_{frap}) was calculated using the following formula:

$$K_{\text{frap}} = C_1 K_{\text{off1}}$$

ix. *Omecamtiv Mecarbil*

Omecamtiv Mecarbil (Selleckchem, Houston, TX) concentrate was prepared as documented by previous publications (Shen 2010) and was used at a 200 nM concentrate. For acute dosing, before experiments, one hour of incubation and activation time was allotted. For continuous dosing, iPSC-CMs were treated with Omecamtiv Mecarbil at the initial time of cell-seeding, and incubated with the activator. These dishes were dosed again each time the media was exchanged every other day until used for experimentation.

x. *Statistical Analysis*

Data was organized using Excel software (Microsoft, Redmond, CA) and statistical analysis was performed using GraphPad Prism (GraphPad Software, La Jolla, CA). Significant differences in variables were determined by using either two-tailed Student's t-test or n-way ANOVA. All data were expressed as mean \pm standard error of the mean. For FRAP assays, the sample number was defined as individual cells, of which one to three cells were analyzed per culture in at least three separate cultures analyzed per experimental condition.

C. Results

i. *iPSC-CM Structure as a Function of Time after Replating*

Immunohistochemistry images show the first stages of development after thawing and plating. Cells were fixed and stained for actin, α -actinin, and the nucleus. At one week, normal iPSC-CMs have well-developed striations, whereas the mutation cells were less organized with fewer striations (Figure 13). At two weeks, both the normal and mutation cells were less organized than at week 1, and the mutation cells had very little to no striation (Figure 14).

ii. *Beating Frequency*

Using brightfield microscopy, beat rate in both the normal and cTnT R173W point mutation iPSC-CMs groups were observed and recorded. At one week, the normal group beat at a rate of 15.8 ± 0.9 (n=15) beats per minute, which was statistically higher than the mutation group rate of 10.8 ± 0.81 beats per minute (n=13) ($p < 0.001$) (Figure 15). At week 2, the control group beat at a rate of 14.9 ± 1.2 (n=19) BPM, and the mutation group beat rate was 16.3 ± 3.3 (n=21) BPM (Figure 15). The BPM in the mutation group was significantly increased from Week 1 to Week 2 ($p = 0.04$).

iii. *Shortening and Shortening Velocity of iPSC-CMs*

The maximum shortening of iPSC-CMs were calculated using a kymograph. At one week of maturation, the average shortening was 0.88 ± 0.04 μm (n=41) in the normal group, and 0.47 ± 0.03 μm (n=36) μm in the mutation group ($p < 0.0001$) (Figure 16). At week 2 of maturation

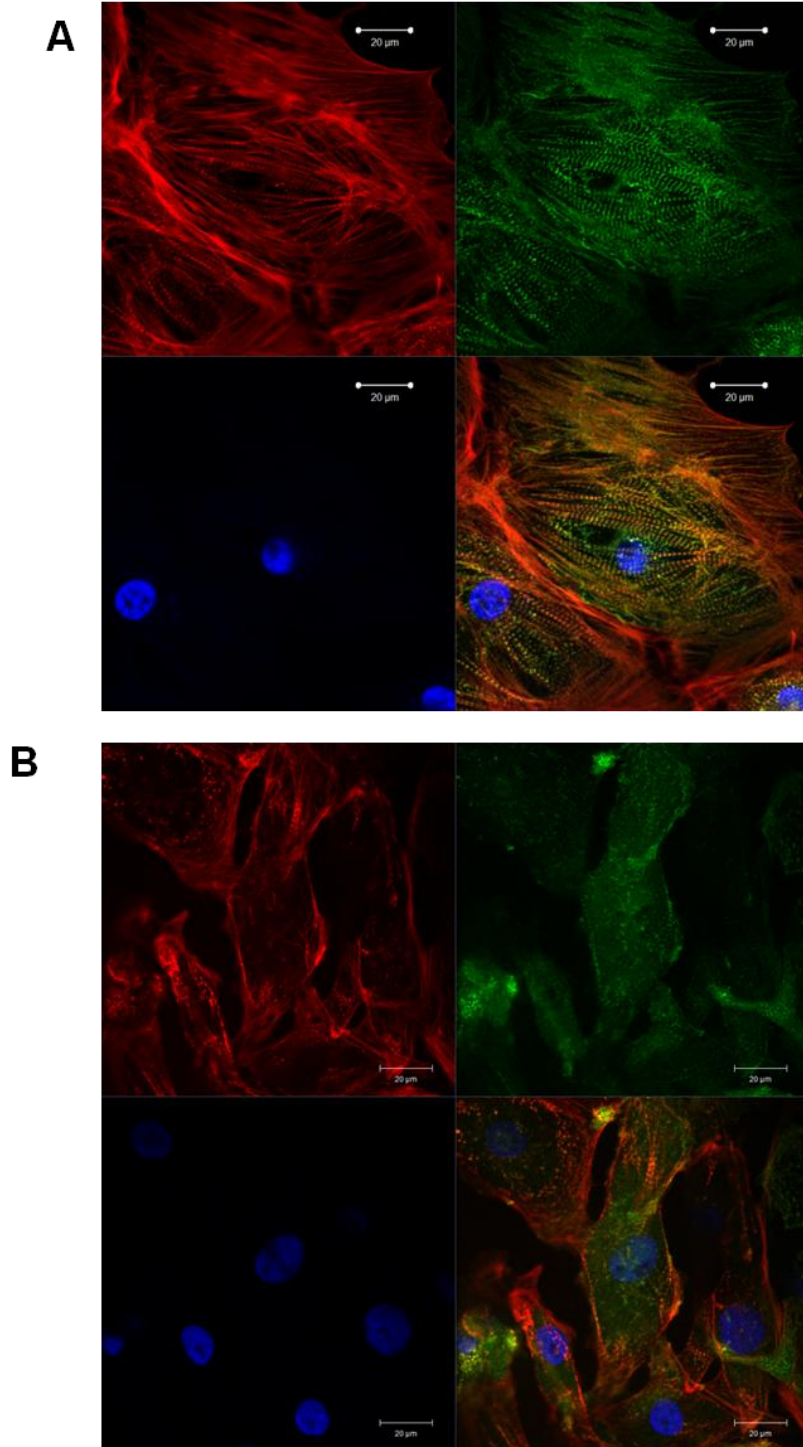


Figure 13: iPSC-CM Maturation at Week 1 in Normal and cTnT R173W Mutation Cells. At 1 week after plating, iPSC-CMs were fixed and stained for sarcomeric alpha-actinin (red), actin (green), and nucleus (DAPI, blue) in both normal and mutant dishes. (a) At one week, normal iPSC-CMs have begun to form well-organized striations of the sarcomere. (b) Mutation iPSC-CMs at one week are less organized and have fewer striations. In collaboration with Jieli Li, MD, PhD.

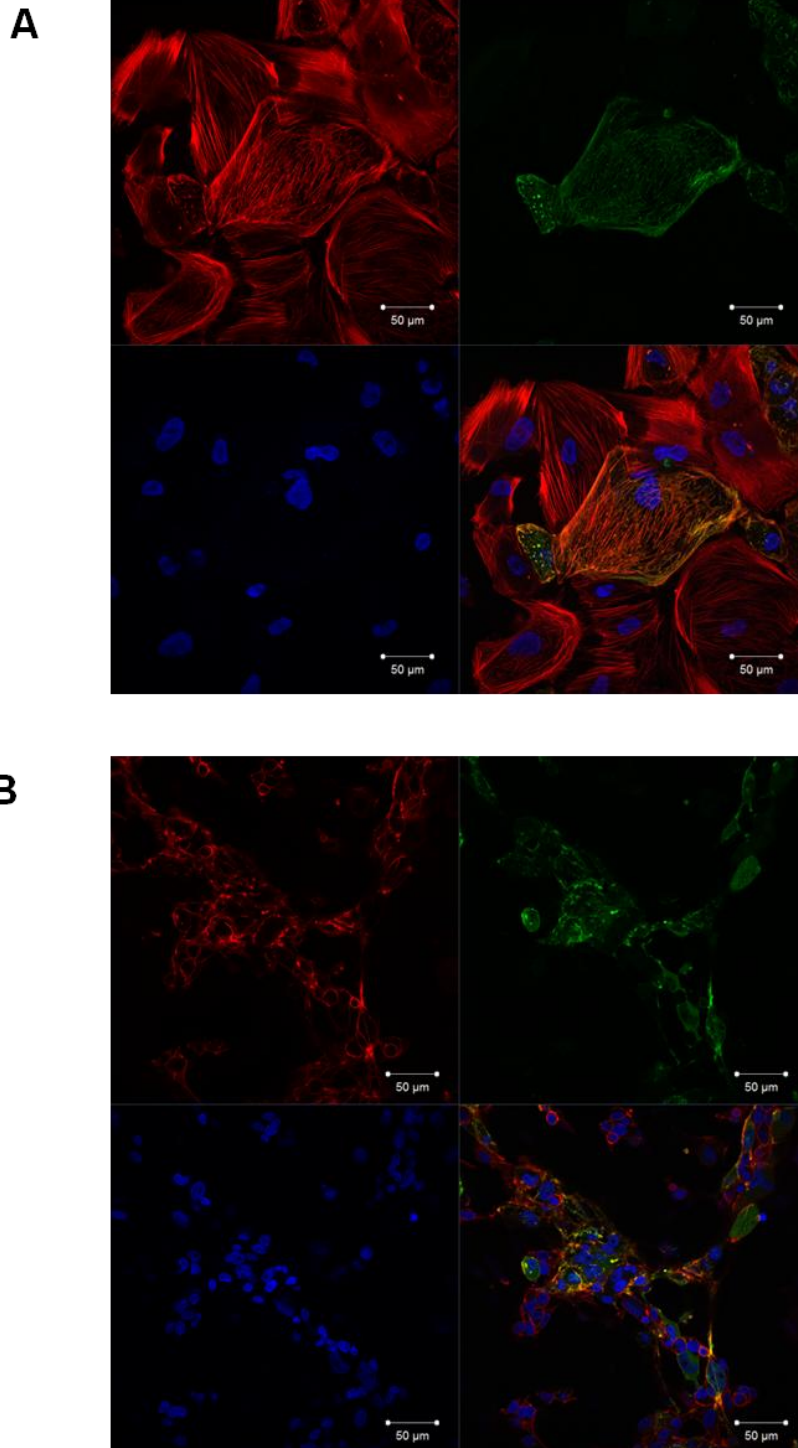


Figure 14: iPSC-CM Maturation at Week 2 in Normal and cTnT R173W Mutation Cells. At 2 weeks days after plating, iPSC-CMs were fixed and stained for sarcomeric alpha-actinin (red), actin (green), and nucleus (DAPI, blue) in both normal and mutant dishes. (a) At Week 2, normal iPSC-CMs have irregular striations and less organization than at Week 1. (b) Mutation iPSC-CMs at Week 1 are disorganized and are not striated. In collaboration with Jieli Li, MD, PhD.

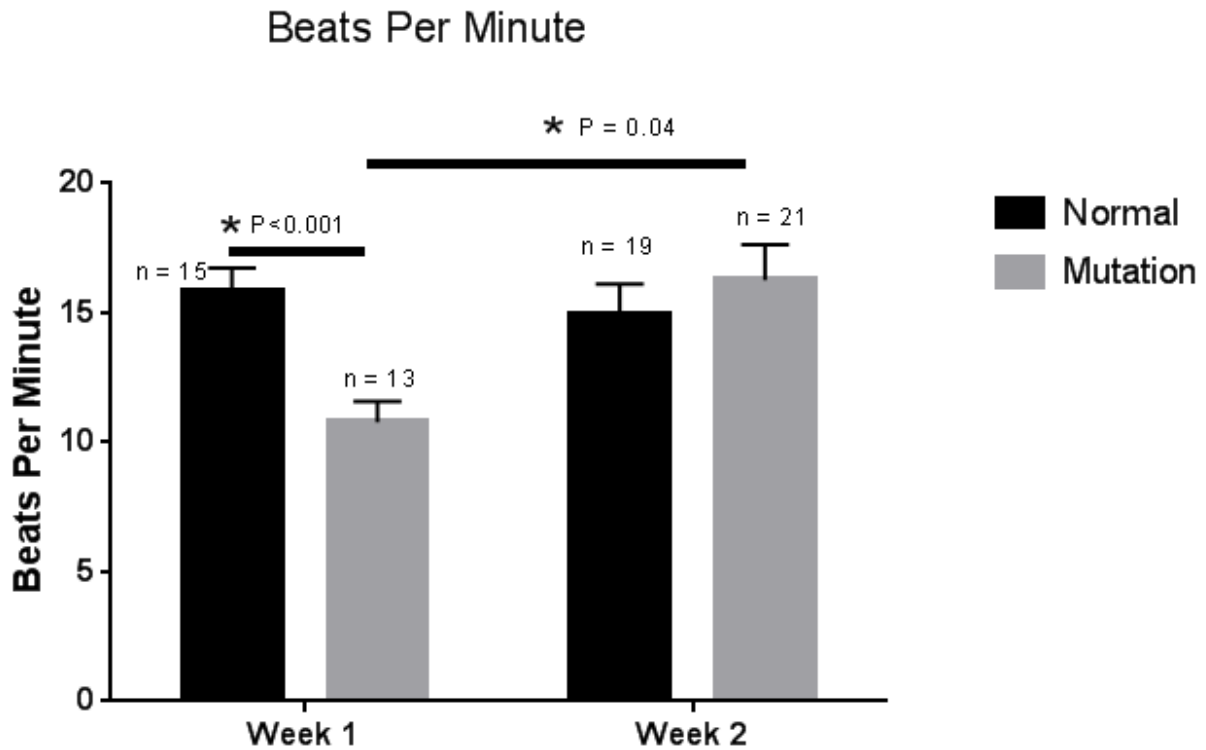


Figure 15: Normal and Mutation iPSC-CMs have Similar Beating Rates by Week 2. The beats per minute of mutation cells were significantly less at Week 1 ($P < 0.001$), however at Week 2, beat rate was in the same range for normal and mutation cells. In collaboration with Kathleen Broughton, PhD.

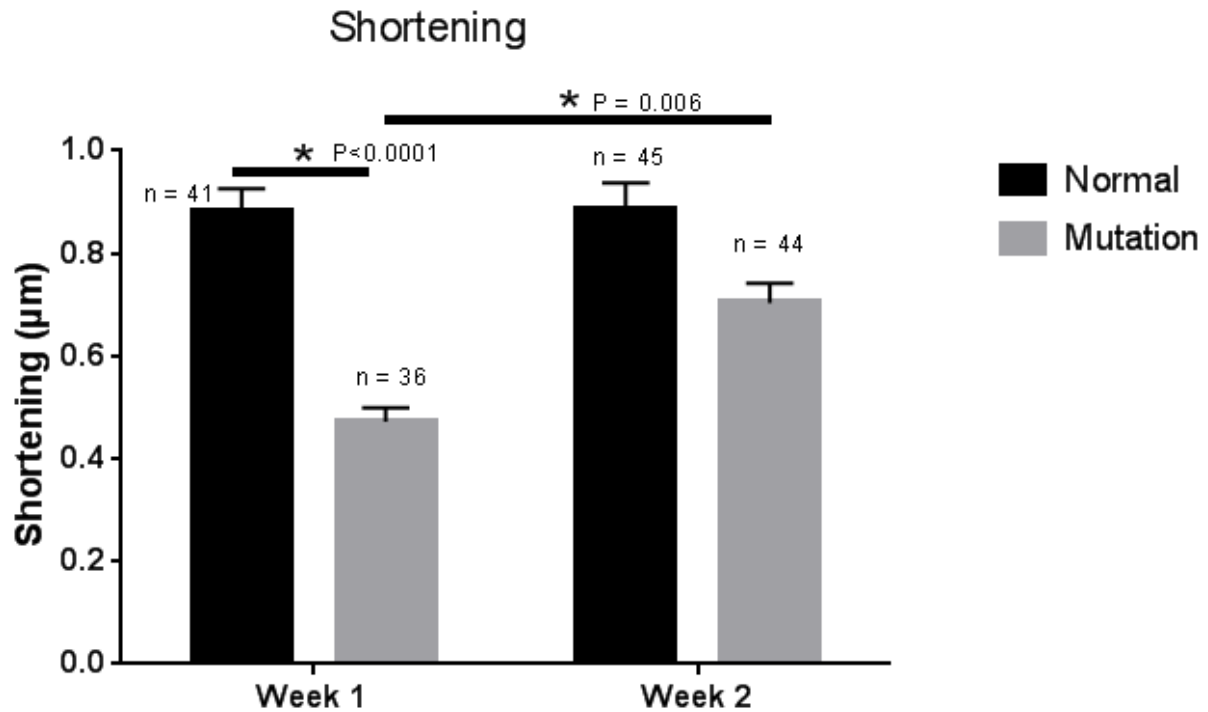


Figure 16: Maximum Shortening of Normal and Mutation iPSC-CMs is Similar by Two Weeks. At week 1 after plating, normal iPSC-CMs have a greater maximum shortening than mutation iPSC-CMs ($p < 0.0001$). At 2 weeks after plating, the maximum shortening of the mutation cells have caught up to the normal iPSC-CMs ($p = 0.006$). In collaboration with Kathleen Broughton, PhD.

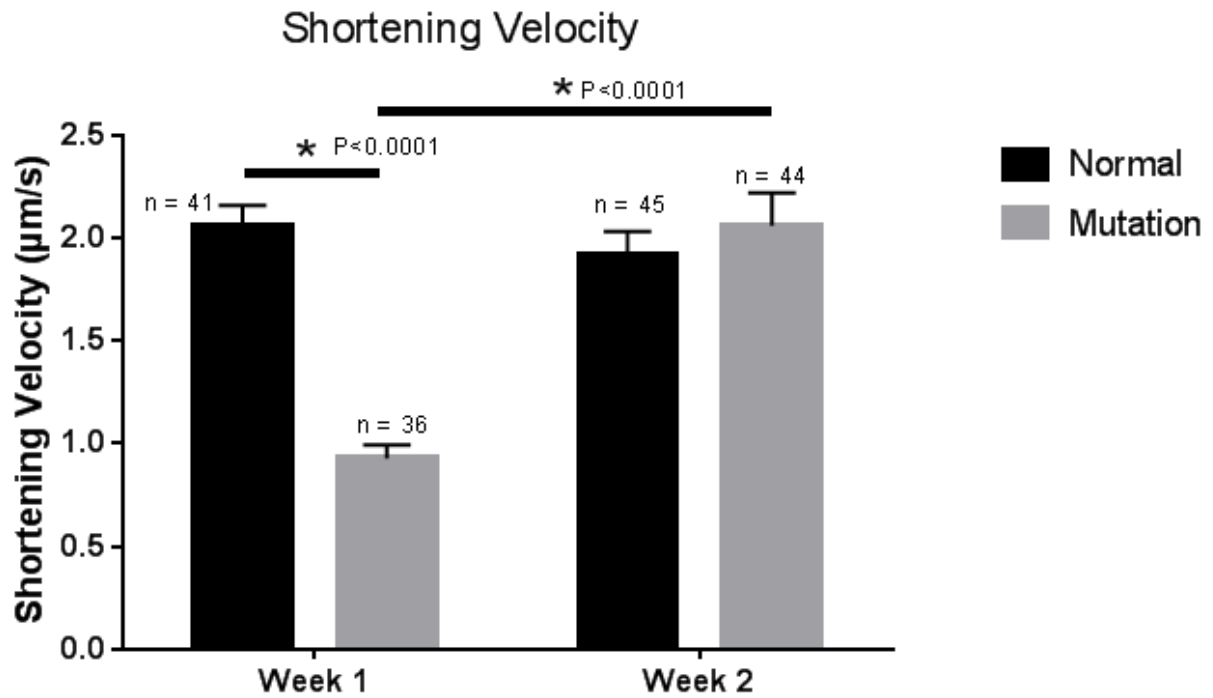


Figure 17: Maximum Shortening Velocity of Normal and Mutation iPSC-CMs as a Function of Maturation. At one week after plating, normal iPSC-CMs have a greater maximum shortening velocity than mutation iPSC-CMs ($p<0.0001$). At 2 weeks after plating, the maximum shortening velocity of the mutation cells have caught up to the normal ($p<0.0001$). In collaboration with Kathleen Broughton, PhD.

maturation, the average shortening was 0.89 ± 0.05 (n=36) μm in the normal group, and 0.70 ± 0.04 μm (n=44) in the mutation group (Figure 16). Shortening was significantly higher at week 2 than at week 1 in the mutant group ($p = 0.0062$). The associated shortening velocity at week 1 was 2.06 ± 0.10 $\mu\text{m/s}$ for normal group (n=41), and 0.93 ± 0.12 $\mu\text{m/s}$ (n=36) for mutation ($p < 0.0001$) (Figure 17). The associated shortening velocity at week 2 was 1.91 ± 0.07 $\mu\text{m/s}$ (n=45) for normal, and 2.06 ± 0.16 $\mu\text{m/s}$ (n=44) for mutation (Figure 17).

iv. *Actin FRAP Dynamics in iPSC-CMs*

The dynamics of sarcomeric actin were measured via FRAP. The cells were infected with actin-GFP fusion virus to visualize the striated pattern and quantify the recovery profile of the actin-GFP fluorescence (Figure 18). The kinetic constant (K_{FRAP}) obtained from the results of the curve fitting were $5.94 \times 10^{-4} \pm 0.0001$ (n=6) for normal and $2.66 \times 10^{-4} \pm 3.8 \times 10^{-4}$ (n=9) for mutation at week 1, which are significantly different ($p=0.02$) (Figure 19). However, at week 2, the kinetic constant (K_{FRAP}) obtained from the results of the curve fitting were $3.73 \times 10^{-4} \pm 8 \times 10^{-5}$ (n=6) for normal and $4.04 \times 10^{-4} \pm 6.1 \times 10^{-5}$ (n=7) mutation, which were not significantly different (Figure 19).

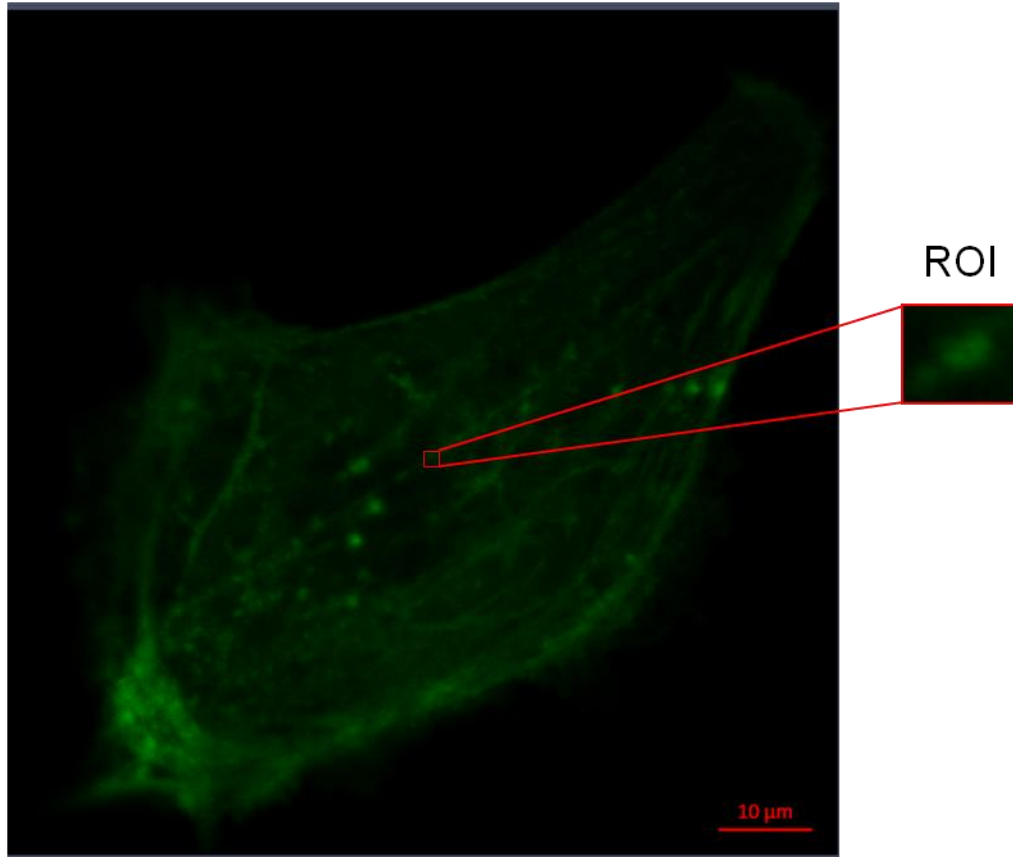


Figure 18: iPSC-CM infected with Actin-GFP for FRAP Experiments. Confocal image to show the localization of actin throughout the cell, as striations are beginning to form. Red box denotes Region of Interest (ROI) of a faint striation in which FRAP was analyzed.

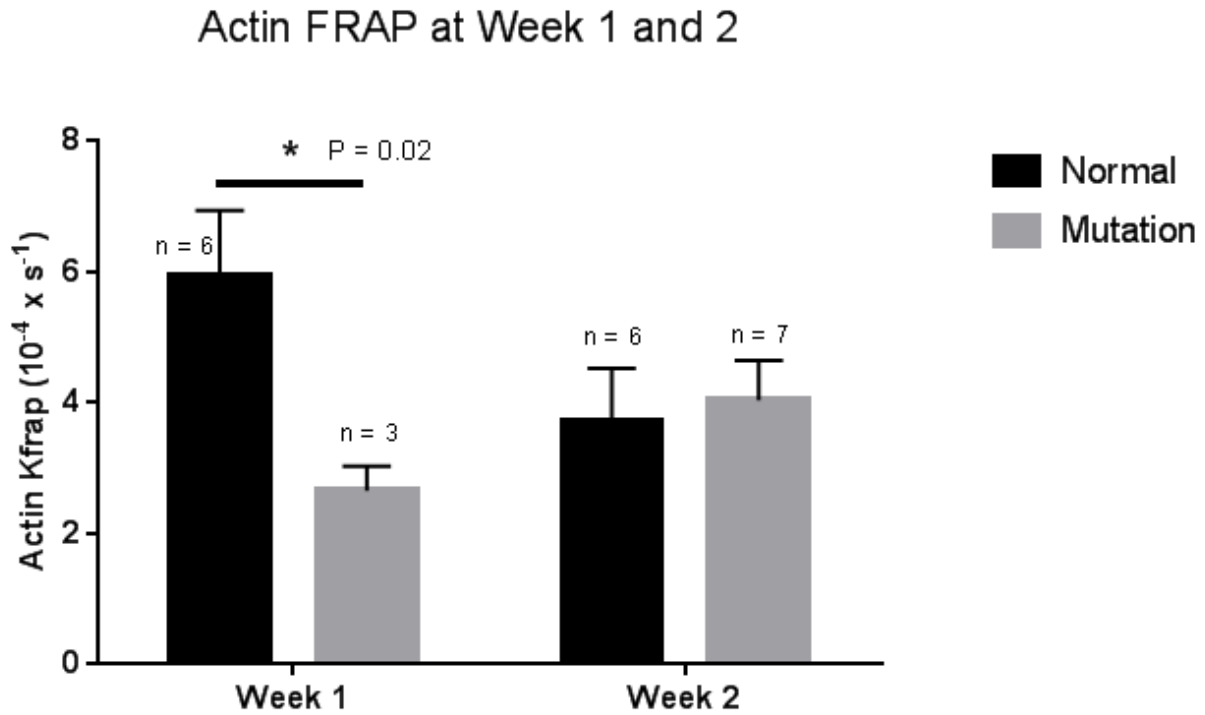


Figure 19: Actin FRAP Dynamics in Mutation iPSC-CMs are Different at Week 1, but Similar to Normal iPSC-CMs by Week 2. Protein dynamic exchange rate is significantly lower in mutation cells than normal iPSC-CMs ($p < 0.02$) at Week 1. By Week 2, actin dynamics in the mutation group are in the same range as the normal group. In collaboration with Ying-Hsi Lin.

v. *Effects of Omecamtiv Mecarbil at One Week after Plating*

iPSC-CM were treated with acutely and chronically with 200 nM Omecamtiv Mecarbil. When untreated, the normal group beat at a rate of 15.8 ± 0.94 (n=15) beats per minute, and the mutation group had a rate of 10.8 ± 0.81 beats per minute (n=13) (Figure 20). With an acute dosage of 200 nM Omecamtiv Mecarbil, the normal group BPM was 14.53 ± 1.1 (n=14) and the mutation group BPM was 14.58 ± 1.9 (n=9) (Figure 20). The cells were also treated continuously, which resulted in a BPM of 11.43 ± 1.5 (n=14) for the normal group, and 11.6 ± 0.9 (n=8) for the mutation group (Figure 20). Although the mutation group shows a trend for a difference between untreated and acute treatments, this difference was not significant.

Omecamtiv Mecarbil acutely applied at a 200 nM concentration to the normal and mutant groups at one week after plating showed a maximum shortening at 0.93 ± 0.06 μm (n=12) compared to the mutation at 0.42 ± 0.04 μm (n=10) in the mutation group (Figure 21). When a 200 nM dose of Omecamtiv Mecarbil was applied chronically, the maximum shortening was 0.96 ± 0.04 μm (n=13) for normal, and 0.59 ± 0.05 μm (n=9) (Figure 21). The corresponding shortening velocities for the acute treatment were 1.72 ± 0.14 $\mu\text{m/s}$ (n=12) and 0.90 ± 0.10 $\mu\text{m/s}$ (n=10) for normal and mutation respectively (Figure 22). With the continuous treatment, the corresponding shortening velocities were 1.75 ± 0.10 $\mu\text{m/s}$ (n=13) and 1.24 ± 0.11 $\mu\text{m/s}$ (n=9) for normal and mutation, respectively (Figure 22).

vi. *Effects of Omecamtiv Mecarbil at Two Weeks after Plating*

At Week 2 after plating, iPSC-CMs were also treated with acutely and chronically with 200 nM Omecamtiv Mecarbil. The maximum shortening was calculated to be 1.14 ± 0.06 μm (n=4) compared to 0.74 ± 0.11 μm (n=4) in the mutation group when treated acutely. When a 200 nM dose of Omecamtiv Mecarbil was applied chronically, the maximum shortening was

$1.21 \pm 0.13 \mu\text{m}$ (n=3) for normal, and $0.85 \pm 0.15 \mu\text{m}$ (n=3) (Figure 23). The corresponding shortening velocities for the acute treatment were $1.28 \pm 0.18 \mu\text{m/s}$ (n=4) and $4.10 \pm 0.33 \mu\text{m/s}$ (n=4) for normal and mutation respectively (Figure 24). With the continuous treatment, the corresponding shortening velocities were $1.95 \pm 0.27 \mu\text{m/s}$ (n=13) and $3.08 \pm 0.11 \mu\text{m/s}$ (n=3) for normal and mutation, respectively, with respect to Omecamtiv Mecarbil therapy (Figure 24). Normal cells showed a significant decrease in velocity in when treated with acute ($p = 0.004$) and chronic ($p = 0.05$) Omecamtiv Mecarbil.

vii. *Actin FRAP Dynamics in iPSC-CMs with Omecamtiv Mecarbil*

Actin FRAP dynamics were measured at weeks 1 and 2 after plating when iPSC-CMs were treated continuously with 200 nM Omecamtiv Mecarbil. At Week 1, the kinetic constant (K_{FRAP}) obtained from the results of the curve fitting was $6.38 \times 10^{-4} \pm 3.3 \times 10^{-5}$ (n=3) for the normal group treated with Omecamtiv Mecarbil (Figure 25). No significant differences were found with Omecamtiv Mecarbil therapy. The mutation group treated with Omecamtiv Mecarbil did not contain sufficient, infected, striated cells for FRAP analysis at Week 1.

Actin FRAP dynamics were also measured at Week 2 when iPSC-CMs were treated continuously with 200 nM Omecamtiv Mecarbil. The kinetic constant (K_{FRAP}) obtained from the results of the curve fitting was $4.07 \times 10^{-4} \pm 8.30 \times 10^{-5}$ (n=2) for the normal group treated with Omecamtiv Mecarbil (Figure 25). The mutation group treated with Omecamtiv Mecarbil had an average K_{FRAP} value of $2.80 \times 10^{-4} \pm 5.6 \times 10^{-5}$ (n=4). No significant differences were observed with the treatment of Omecamtiv Mecarbil.

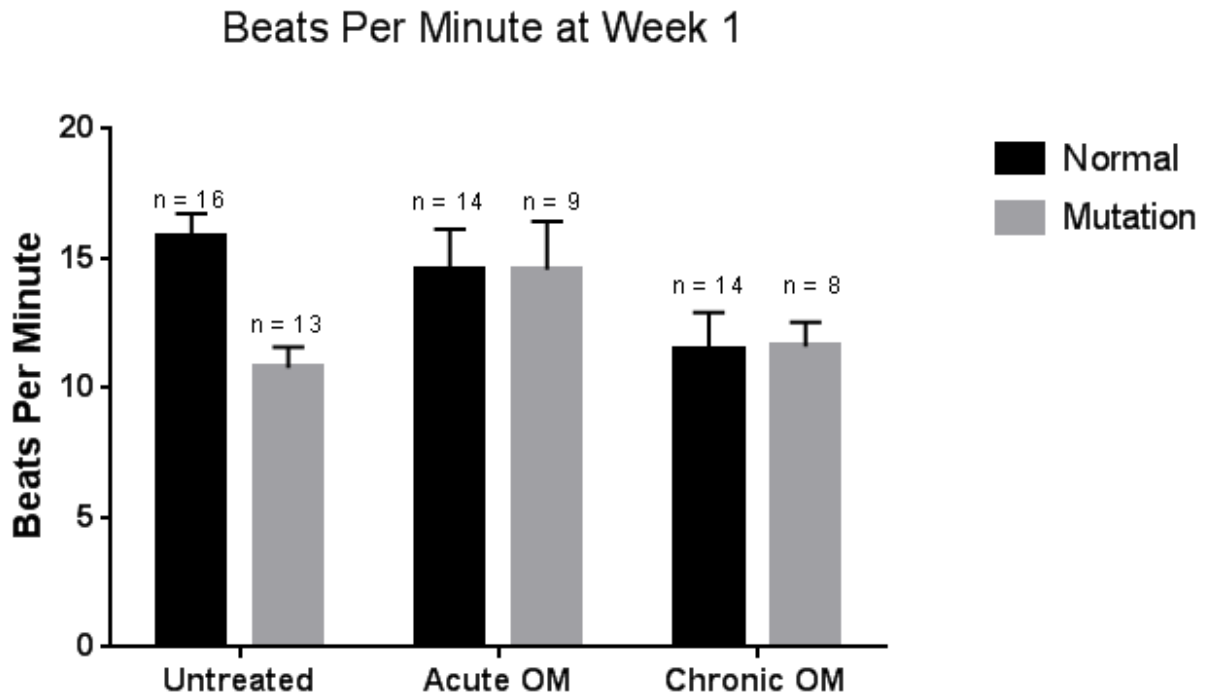


Figure 20: Normal and Mutation iPSC-CMs Beats per Minute are not Significantly Different when Treated with 200 nM Omecamtiv Mecarbil at Week 1. Human iPSC-CMs were measured for beats per minute when untreated, treated acutely, or treated continuously at Week 1 from the time of plating with the 200 nM of myosin activator Omecamtiv Mecarbil. Beats per minute of the normal and mutation iPSC-CMs were not significantly different by acute or continuous treatment. In collaboration with Kathleen Broughton, PhD.

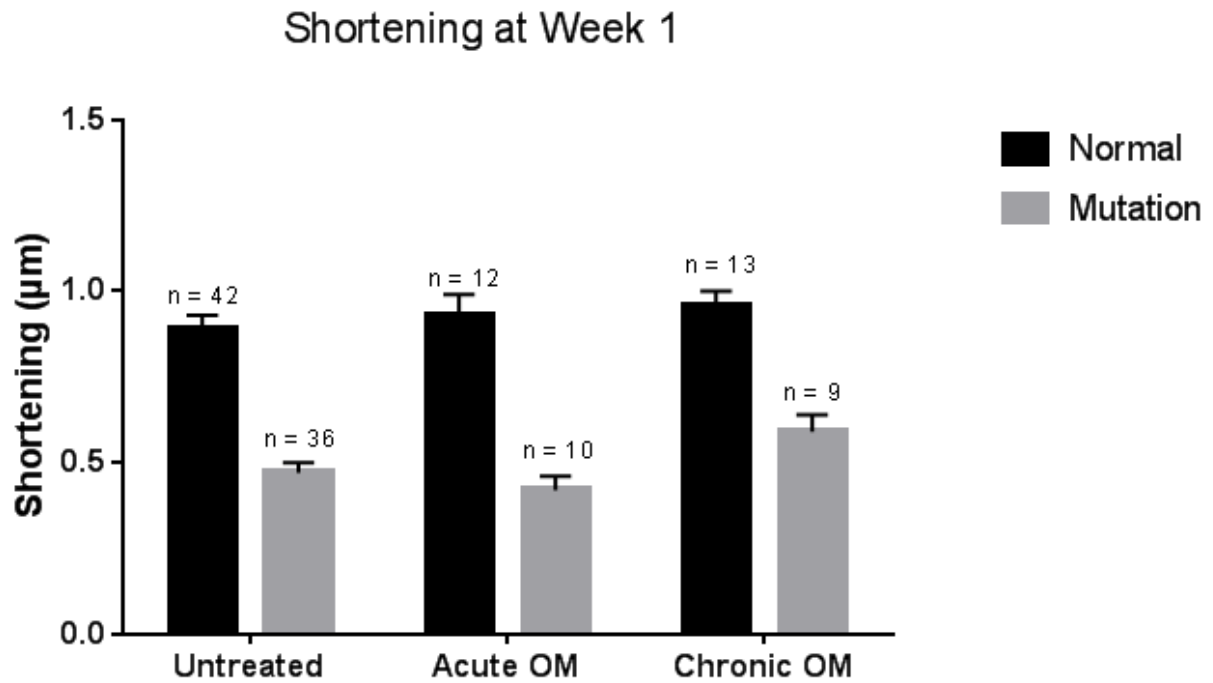


Figure 21: Normal and Mutation human iPSC-CMs Shortening Properties are not Significantly Different when Acutely or Continuously Treated with 200 nM Omecamtiv Mecarbil at Week 1. Maximum shortening does not affect normal or mutation iPSC-CMs when acutely or continuously treated with 200 nM Omecamtiv Mecarbil. In collaboration with Kathleen Broughton, PhD.

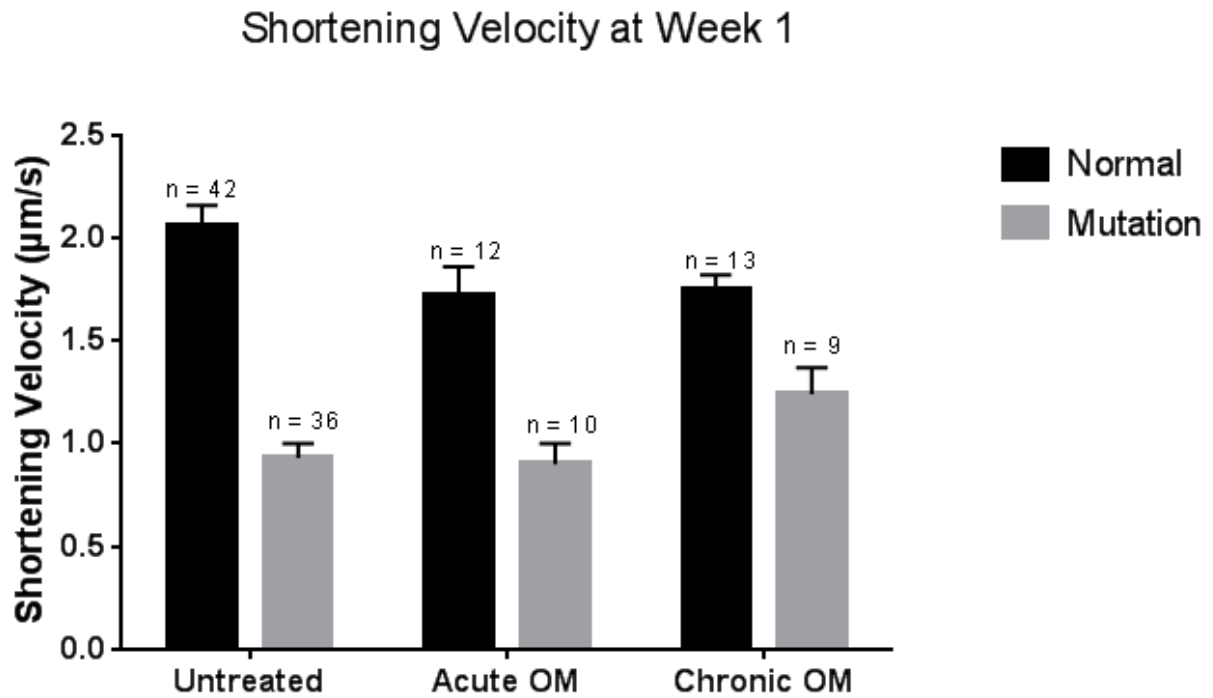


Figure 22: Normal and Mutation human iPSC-CMs Shortening Velocity are not Significantly Different when Acutely or Continuously Treated with 200 nM Omecamtiv Mecarbil at Week 1. Maximum shortening velocity was not affected in normal or mutation iPSC-CMs by acute or continuous treatment of 200 nM Omecamtiv Mecarbil. In collaboration with Kathleen Broughton, PhD.

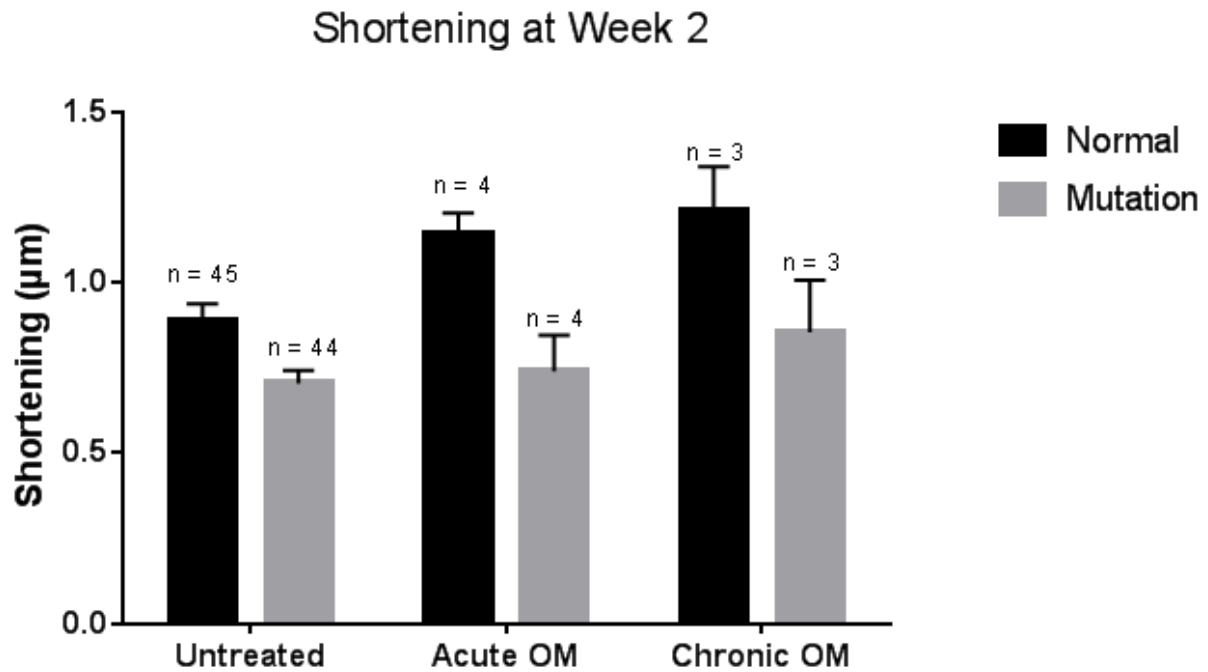


Figure 23: Normal and Mutation human iPSC-CMs Shortening Properties are not Significantly Different when Acutely or Continuously Treated with 200 nM Omecamtiv Mecarbil at Week 2. Maximum shortening is not affected by a 200 nM dose of Omecamtiv Mecarbil in normal or mutation iPSC-CMs.

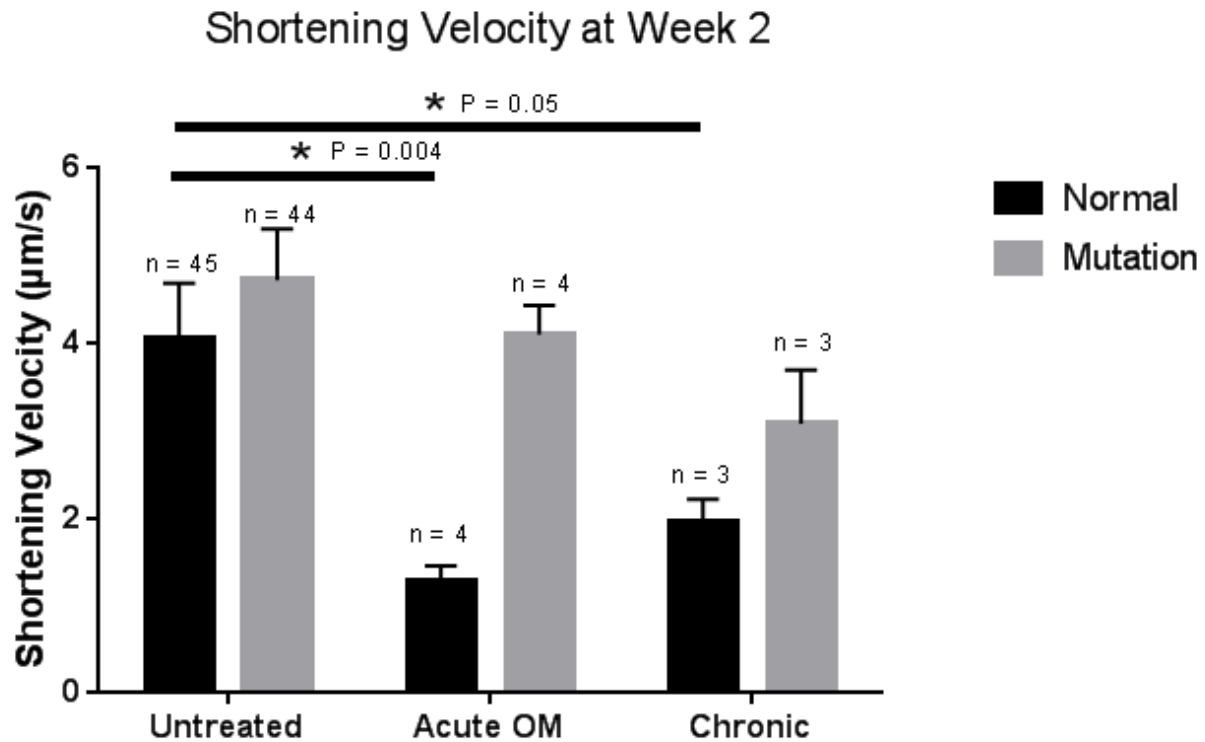


Figure 24: Normal and Mutation human iPSC-CMs Shortening Velocity is Decreased with Acute or Continuous Treatments of 200 nM Omecamtiv Mecarbil at Week 2. Maximum shortening velocity was decreased in normal iPSC-CMs when acutely or continuously treated with 200 nM Omecamtiv Mecarbil. There was no significant difference in the mutation group shortening velocity with the acute or chronic Omecamtiv Mecarbil treatment.

Actin FRAP with OM

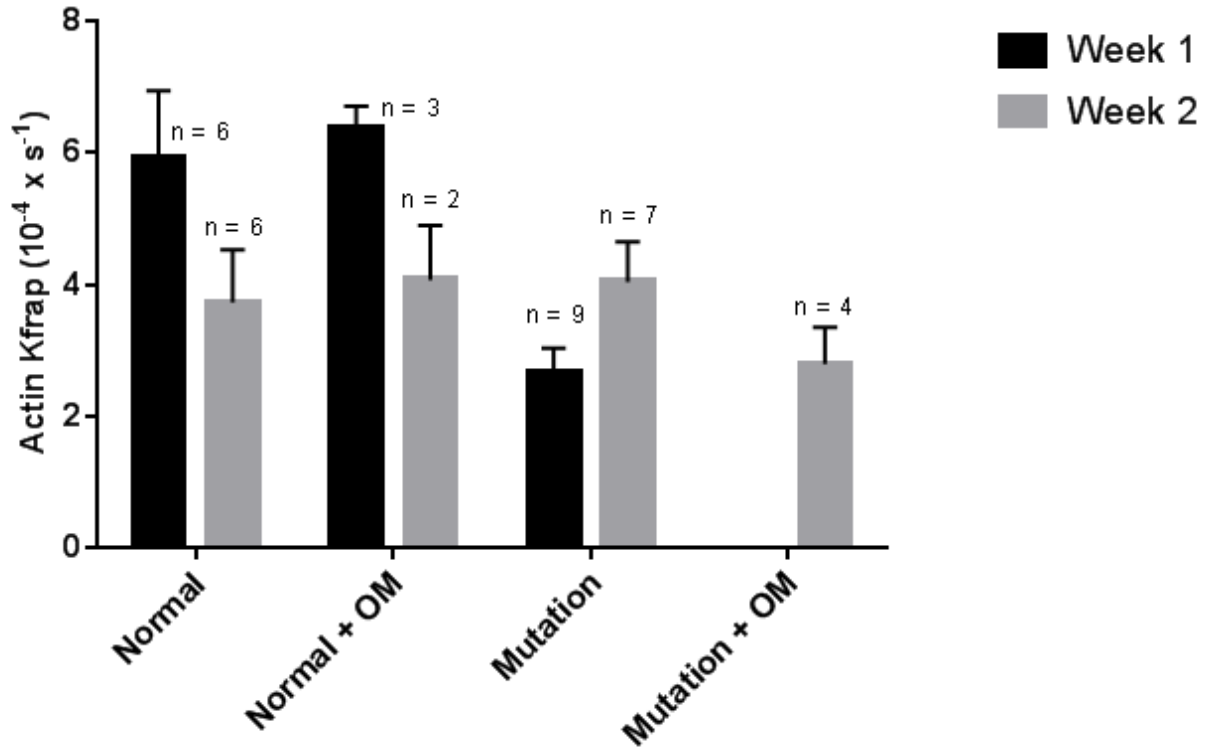


Figure 25: Actin-FRAP Dynamics in Normal and Mutation human iPSC-CMs when Treated with 200 nM Omecamtiv Mecarbil. Chronic Treatment of 200 nM Omecamtiv Mecarbil does not rescue actin FRAP dynamics in normal or mutation cells. In collaboration with Ying-Hsi Lin.

D. Discussion

This study demonstrates the structure and function of normal iPSC-CMs differ from DCM iPSC-CMs plated on soft substrates (100 kPa PDMS). Previous studies have used stiffer surfaces (Sun 2012). The number of days post cell plating played a big role in the functional maturation of iPSC-CMs. At the early stages of maturation, the mutation cells are significantly less organized in terms of sarcomere structure than the normal cells, which correlates with less contractility and reduced actin assembly dynamics. By the later stages of maturation, the mutation cells have developed to match the physiological range of the normal cells in terms of shortening, velocity, and actin assembly.

The use of biocompatible substrates influenced the maturation of both normal and DCM iPSC-CMs. This study showed that normal iPSC-CMs were able to begin spontaneous contraction within the first week after plating, which is consistent with previous studies (Sun 2012). Plating the iPSC-CMs on PDMS substrates with a stiffness of 100 kPa was physiologically similar to heart tissue as compared to the very stiff glass substrates (1 GPa) (Berry 2006; Discher 2005; Nemir 2009). Cardiomyocyte performance has been previously shown to be affected by the substrate stiffness, with the softer surfaces showing decreased contractility (Engler 2008; Jacot 2008).

It has been demonstrated in previous studies that the Troponin T complex is an important regulator for both contraction and sarcomere assembly (Ferrante 2010). By disrupting the expression of different troponin T genes in zebrafish, it was demonstrated that losing the regulation of actin-myosin activity leads to sarcomere assembly failure. Not only is troponin required for actin-myosin interactions, it also affects myofibrillogenesis of the proper thin filament assembly. When mutant troponin T thin filaments were present, the assembly was

underdeveloped, and immature sarcomeres were formed. Given these findings, it is possible that contractility feeds back on assembly, as shown in the second chapter of this thesis. Therefore in this study, the use of Omecamtiv Mecarbil was implemented, in hopes that it could rescue the contractility and rescue the delayed sarcomere assembly of mutation iPSC-CMs.

Using a normal iPSC-CM compared to a DCM iPSC-CM line showed a functional method to study disease and explore possible therapies for afflicted patients. Although the 200 nM dose of Omecamtiv Mecarbil did not alter the sarcomeric function of iPSC-CMs, its known ability to sensitize myofilaments suggests that a higher dose might be effective (Shen 2010; Malik 2011). The findings presented here showed similar contractile dysfunction and disorganization of the cTnT R173 point mutation iPSC-CMs as previously described (Sun 2012). This may be due to the fact that at the cellular level, DCM models have shown to be more likely influenced by mechanical stress, which may affect sarcomeric organization (Arber 1997; Hassel 2009). In this case, because iPSC-CMs were plated on 100 kPa substrates, mechanical cues may have had a larger influence on sarcomere development than did Omecamtiv Mecarbil, since it is known that mechanical load feeds back to sarcomere assembly (Russell 2010).

Decreased shortening and shortening velocity, as well as decreased actin dynamics in DCM iPSC-CMs in this study are related to the findings of other studies that examined contractility and force generation of DCM iPSC-CMs (Sun 2012). This shows DCM linked mutations have decreased force, shortening, and sarcomere assembly capabilities that result in an altered phenotype, which leads to dysfunctional signaling within the cell.

E. Conclusion

Point mutations can serve as a major contributing factor to cardiomyopathy by causing disruption in the structure and function of the sarcomere. Thin filaments also play a major role of regulating mechanics in the sarcomere. To further understand and investigate point mutations, iPSC-CMs are a great tool to create models for treating cardiovascular disease.

The structure and function of cTnT R173W mutation iPSC-CMs matured at a slower rate than the normal iPSC-CMs, suggesting that sarcomeric assembly is also slower in the mutation cells. Omecamtiv Mecarbil was used to test whether myofibril assembly could be improved by sensitizing the myofilament. However, at the 200 nM dose, it had no significant effect on the shortening properties and actin dynamics. Future studies can be conducted to use a higher dosage of Omecamtiv Mecarbil or other drugs. There are many other point mutations that lead to similar myopathies, which could be used as a platform for micromechanical analysis and discovery for potential drug treatments.

IV. Conclusions

A. Major Findings

The major findings from the experiments of this study are outlined as follows:

Chapter II: Subcellular Contractility and Actin Assembly as Influenced by 3D Microtopography in Neonatal Rat Ventricular Myocytes

1. BioMEMs devices can be constructed with desired microtopography surfaces and stiffness to mimic cardiac muscle cells
2. NRVMs plated on microtopography surfaces exhibit higher shortening and shortening properties than NRVMs plated on flat surfaces.
3. Maximum shortening was found in the middle region of an NRVM anchored to a 3D micropost, as compared to the region near the post and the region furthest away from the post.
4. NRVMs plated on microtopography surfaces exhibit higher actin dynamics than NRVMs plated on flat surfaces.
5. Higher actin dynamics were exhibited on an NRVM region anchored near the post, followed by the mid-region of the cell, and the far-region of the cell.
6. The fraction of PKC- ϵ on an NRVM attached to the post was highest in the region near the post, and lowest far away from the post.

Chapter III: Sarcomere Structure and Assembly in Normal Human and cTnT Mutation Cardiomyocytes Derived from Induced Pluripotent Stem Cells

7. iPSC-CMs are a useful tool to model patient-specific diseases.
8. cTnT R173W mutation in iPSC-CMs demonstrate less organized sarcomere structure than normal iPSC-CMs at both weeks 1 and 2.
9. Mutation iPSC-CMs show smaller shortening and shortening velocity at week 1 after plating than normal iPSC-CMs.
10. Mutation and normal iPSC-CMs show similar shortening and shortening velocity at week 2.
11. Mutation iPSC-CMs have significantly lower actin dynamics than normal iPSC-CMs at week 1.
12. Normal and Mutation iPSC-CMs show similar actin dynamics at week 2 after plating.
13. Omecamtiv Mecarbil does not show any significant effect on normal or mutation iPSC-CMs when dosed acutely or chronically at 200 nM in the beat frequency, shortening, or shortening velocity at week 1 after plating.
14. Omecamtiv Mecarbil does not show any significant effect on normal or mutation iPSC-CMs when dosed acutely or chronically at 200 nM in the beat frequency or shortening at week 2 after plating.
15. Omecamtiv Mecarbil decreases shortening velocity in normal iPSC-CMs when dosed acutely and chronically at 200 nM concentrate.
16. Actin dynamics are not affected by 200 nM Omecamtiv Mecarbil in normal or mutation iPSC-CMs at weeks 1 or 2.

B. Significance

The use of bioengineering techniques, such as BioMEMS device fabrication, provides a unique approach for micromechanical analysis of cardiomyocytes. The studies demonstrate useful tools and methods to mimic cardiac physiology for application in a complex, biomechanical system. Studying cardiomyocytes on 3D microtopography substrates can advance current strategies in clinical applications, such as regenerative medicine. The use of human induced pluripotent stem cell derived cardiomyocytes offers a useful model for studying cardiac disease. By using these cells, individualized treatments for myopathy caused by single point mutations can be developed. Finally, the drug Omecamtiv Mecarbil provides insight into a potential treatment for heart failure and motivates further the further study of its effect on the diseased heart.

C. Future Directions

This thesis has yielded several opportunities for future research. The experiments in the first section demonstrate a useful model for studying cardiomyocyte response to external mechanical stress. To advance the understanding of the force generation relationship in cardiomyocytes, further studies can be conducted to build better 3D models that utilize different microtopography patterns, such as microgrooves, to accurately describe contractility and assembly in heart muscle.

The experiments from the second section of this thesis highlight the use of bioengineering techniques to characterize normal and diseased iPSC-CMs. Although the use of Omecamtiv Mecarbil did not significantly improve the function of mutation iPSC-CMs, a next step would be to test the drug using a higher dosage to test whether it has the potential to rescue diseased iPSC-CMs to the normal state. In all, this study offers relevant information and useful tools to study heart disease, and provides insight to the treatment of patients suffering from heart disease.

V. Cited Literature

1. Alberts B, Johnson A, Lewis J, Raff M, Roberts K, Walter P. The Cytoskeleton. *Molecular Biology of the Cell*. 5th edition. 2008;16:965-1052
2. Arber, S., Hunter, J. J., Ross Jr, J., Hongo, M., Sansig, G., Borg, J., ... & Caroni, P. (1997). MLP-deficient mice exhibit a disruption of cardiac cytoarchitectural organization, dilated cardiomyopathy, and heart failure. *Cell*,88(3), 393-403.
3. Baker, M. (2007). Adult cells reprogrammed to pluripotency, without tumors. *Nature Reports Stem Cells*.
4. Basta P, Strickland MB, Holmes W, Loomis CR, Ballas LM, Burns DJ (Nov 1992). "Sequence and expression of human protein kinase C-epsilon". *Biochim Biophys Acta* 1132 (2): 154-60
5. Berry MF, Engler AJ, Woo YJ, Pirolli TJ, Bish LT, Jayasankar V, Morine KJ, Gardner TJ, Discher DE, Sweeney HL (2006) Mesenchymal stem cell injection after myocardial infarction improves myocardial compliance *Am J Physiol Heart Circ Physiol* 290(6):H2196-203.
6. Boateng, S. Y., Hartman, T. J., Ahluwalia, N., Vidula, H., Desai, T. A., & Russell, B. (2003). Inhibition of fibroblast proliferation in cardiac myocyte cultures by surface microtopography. *American Journal of Physiology-Cell Physiology*, 285(1), C171-C182.
7. Broughton, K. M., & Russell, B. (2014). Cardiomyocyte subdomain contractility arising from microenvironmental stiffness and topography. *Biomechanics and modeling in mechanobiology*, 1-14.
8. Brutsaert, D. L., & Sonnenblick, E. H. (1969). Force-velocity-length-time relations of the contractile elements in heart muscle of the cat. *Circulation research*, 24(2), 137-149.

9. Burridge, PW, Diecke, S., Matsa, E., Sharma, A., Wu, H., & Wu, J. C. (2014). Modeling Cardiovascular Diseases with Patient-Specific Human Pluripotent Stem Cell-Derived Cardiomyocytes. *Methods in Molecular Biology*, 10, 7651_2015_196.
10. Chen L, Hahn H, Wu G, Chen CH, Liron T, Schechtman D, Cavallaro G, Banci L, Guo Y, Bolli R, Dorn GW 2nd, Mochly-Rosen D. Opposing cardioprotective actions and parallel hypertrophic effects of delta PKC and epsilon PKC. *Proc Natl Acad Sci U S A*. 2001 Sep 25;98(20):11114-9.
11. Cheng, J., Türkel, N., Hemati, N., Fuller, M. T., Hunt, A. J., & Yamashita, Y. M. (2008). Centrosome misorientation reduces stem cell division during ageing. *Nature*, 456(7222), 599-604.
12. Cheng Q, Sun Z, Meininger G, Almasri M. PDMS elastic micropost arrays for studying vascular smooth muscle cells. *Sensors and Actuators B: Chemical*. 2013;188(0):1055-1063.
13. Curtis, M. W., Budyn, E., Desai, T. A., Samarel, A. M., & Russell, B. (2013). Microdomain heterogeneity in 3D affects the mechanics of neonatal cardiac myocyte contraction. *Biomechanics and modeling in mechanobiology*, 12(1), 95-109.
14. Deng XF, Mulay S, Varma DR. Role of Ca(2+)-independent PKC in alpha 1-adrenoceptor-mediated inotropic responses of neonatal rat hearts. *Am J Physiol*. 1997 Sep;273(3 Pt 2):H1113-8.
15. Disatnik MH, Buraggi G, Mochly-Rosen D. Localization of protein kinase C isozymes in cardiac myocytes. *Exp Cell Res*. 1994 Feb;210(2):287-97.
16. Discher DE, Janmey P, Wang YL (2005) Tissue cells feel and respond to the stiffness of their substrate *Science* 310:1139–1143.

17. Dorn GW 2nd, Mochly-Rosen D. Intracellular transport mechanisms of signal transducers. *Annu Rev Physiol.* 2002;64:407-29. Review.
18. Drumheller, D.L. Ebert, J.A. Hubbell, “Multifunctional poly(ethylene glycol) semi-interpenetrating polymer networks as highly selective adhesive substrates for bioadhesive peptide grafting,” *Biotechnol. Bioeng.* 43(1994):772-780.
19. Duquesnes N, Lezoualc'h F, Crozatier B. PKC-delta and PKC-epsilon: foes of the same family or strangers? *J Mol Cell Cardiol.* 2011 Nov;51(5):665-73.
20. Engler, A. J., Sen, S., Sweeney, H. L., & Discher, D. E. (2006). Matrix elasticity directs stem cell lineage specification. *Cell*, 126(4), 677-689.
21. Ferrante, M. I., Kiff, R. M., Goulding, D. A., & Stemple, D. L. (2011). Troponin T is essential for sarcomere assembly in zebrafish skeletal muscle. *Journal of cell science*, 124(4), 565-577.
22. Flanagan, L. A., Y. E. Ju, B. Marg, M. Osterfield, and P. A. Janmey. Neurite branching on deformable substrates. *Neuroreport* 13:2411–2415, 2002
23. Fuard, D., Tzvetkova-Chevolleau, T., Decossas, S., Tracqui, P., & Schiavone, P. (2008). Optimization of poly-di-methyl-siloxane (PDMS) substrates for studying cellular adhesion and motility. *Microelectronic Engineering*, 85(5), 1289-1293.
24. Gomes, A. V., Barnes, J. A., Harada, K., & Potter, J. D. (2004). Role of troponin T in disease. *Molecular and cellular biochemistry*, 263(1), 115-129.
25. Goody, R. S. (2003). The missing link in the muscle cross-bridge cycle. *Nature Structural & Molecular Biology*, 10(10), 773-775.

26. Hassel, D., Dahme, T., Erdmann, J., Meder, B., Hüge, A., Stoll, M., ... & Rottbauer, W. (2009). Nexilin mutations destabilize cardiac Z-disks and lead to dilated cardiomyopathy. *Nature medicine*, 15(11), 1281-1288.
27. Hazeltine LB, Simmons CS, Salick MR, Lian X, Badur MG, Han W, Delgado SM, Wakatsuki T, Crone WC, Pruitt BL, Palecek SP (2012) Effects of substrate mechanics on contractility of cardiomyocytes generated from human pluripotent stem cells. *Int J Cell Biol* 2012:508294
28. He, J., Ogden, L. G., Bazzano, L. A., Vupputuri, S., Loria, C., & Whelton, P. K. (2001). Risk factors for congestive heart failure in US men and women: NHANES I epidemiologic follow-up study. *Archives of internal medicine*, 161(7), 996-002.
29. Hershberger, R. E., Pinto, J. R., Parks, S. B., Kushner, J. D., Li, D., Ludwigsen, S., ... & Potter, J. D. (2009). Clinical and functional characterization of TNNT2 mutations identified in patients with dilated cardiomyopathy. *Circulation: Cardiovascular Genetics*, 2(4), 306-313.
30. Hill, T. L. (1974). Theoretical formalism for the sliding filament model of contraction of striated muscle Part I. *Progress in biophysics and molecular biology*, 28, 267-340.
31. Hocheng, H., Chen, C. M., Chou, Y. C., & Lin, C. H. (2010). Study of novel electrical routing and integrated packaging on bio-compatible flexible substrates. *Microsystem technologies*, 16(3), 423-430.
32. Huxley, H. E. (1969). The mechanism of muscular contraction. *Science*, 164(886), 1356-1365.
33. Ingber, D.E (2002). Mechanical signaling and the cellular response to extracellular matrix in angiogenesis and cardiovascular physiology. *Circulation research*, 91(10), 877-887.

34. Jacot, J. G., McCulloch, A. D., & Omens, J. H. (2008). Substrate stiffness affects the functional maturation of neonatal rat ventricular myocytes. *Biophysical journal*, 95(7), 3479-3487.
35. Kamisago, M., Sharma, S. D., DePalma, S. R., Solomon, S., Sharma, P., McDonough, B., ... & Seidman, C. E. (2000). Mutations in sarcomere protein genes as a cause of dilated cardiomyopathy. *New England Journal of Medicine*, 343(23), 1688-1696.
36. Kaprielian, R. R., Stevenson, S., Rothery, S. M., Cullen, M. J., & Severs, N. J. (2000). Distinct patterns of dystrophin organization in myocyte sarcolemma and transverse tubules of normal and diseased human myocardium. *Circulation*, 101(22), 2586-2594.
37. Kass, D. A., & Solaro, R. J. (2006). Mechanisms and use of calcium-sensitizing agents in the failing heart. *Circulation*, 113(2), 305-315.
38. Katz, B. (1939). The relation between force and speed in muscular contraction. *The Journal of Physiology*, 96(1), 45.
39. Katz, A. M. (2010). *Physiology of the Heart*. Lippincott Williams & Wilkins.
40. Kobayashi, T., & Solaro, R. J. (2005). Calcium, thin filaments, and the integrative biology of cardiac contractility. *Annu. Rev. Physiol.*, 67, 39-67.
41. LaNasa, S. M., & Bryant, S. J. (2009). Influence of ECM proteins and their analogs on cells cultured on 2-D hydrogels for cardiac muscle tissue engineering. *Acta biomaterialia*, 5(8), 2929-2938.
42. Lee, J. N., Jiang, X., Ryan, D., & Whitesides, G. M. (2004). Compatibility of mammalian cells on surfaces of poly (dimethylsiloxane). *Langmuir*, 20(26), 11684-11691.

43. Lin, Y. H., Li, J., Swanson, E. R., & Russell, B. (2013). CapZ and actin capping dynamics increase in myocytes after a bout of exercise and abates in hours after stimulation ends. *Journal of Applied Physiology*, 114(11), 1603-1609.
44. Lu, Q. W., Morimoto, S., Harada, K., Du, C. K., Takahashi-Yanaga, F., Miwa, Y., ... & Ohtsuki, I. (2003). Cardiac troponin T mutation R141W found in dilated cardiomyopathy stabilizes the troponin T–tropomyosin interaction and causes a Ca²⁺ desensitization. *Journal of molecular and cellular cardiology*, 35(12), 1421-1427.
45. Malik, F. I., Hartman, J. J., Elias, K. A., Morgan, B. P., Rodriguez, H., Brejc, K., ... & Morgans, D. J. (2011). Cardiac myosin activation: a potential therapeutic approach for systolic heart failure. *Science*, 331(6023), 1439-1443.
46. Mansour H, de Tombe PP, Samarel AM, Russell B. Restoration of resting sarcomere length after uniaxial static strain is regulated by protein kinase Cepsilon and focal adhesion kinase. *Circ Res*. 2004 Mar 19;94(5):642-9.
47. McKillop, D. F., & Geeves, M. A. (1993). Regulation of the interaction between actin and myosin subfragment 1: evidence for three states of the thin filament. *Biophysical journal*, 65(2), 693-701.
48. Minamisawa, S., Hoshijima, M., Chu, G., Ward, C. A., Frank, K., Gu, Y., ... & Chien, K. R. (1999). Chronic phospholamban–sarcoplasmic reticulum calcium ATPase interaction is the critical calcium cycling defect in dilated cardiomyopathy. *Cell*, 99(3), 313-322.
49. Mitra, S. K., Hanson, D. A., & Schlaepfer, D. D. (2005). Focal adhesion kinase: in command and control of cell motility. *Nature Reviews Molecular Cell Biology*, 6(1), 56-68.

50. Mogensen, J., Murphy, R. T., Shaw, T., Bahl, A., Redwood, C., Watkins, H., ... & McKenna, W. J. (2004). Severe disease expression of cardiac troponin C and T mutations in patients with idiopathic dilated cardiomyopathy. *Journal of the American College of Cardiology*, 44(10), 2033-2040.
51. Morimoto S, Lu QW, Harada K, Takahashi-Yanaga F, Minakami R, Ohta M, Sasaguri T, Ohtsuki I (2002) Ca-desensitizing effect of a deletion mutation delta K210 in cardiac troponin T that causes familial dilated cardiomyopathy. *Proc Natl Acad Sci U S A*. 99:913–918.
52. Morrison, S. J., & Kimble, J. (2006). Asymmetric and symmetric stem-cell divisions in development and cancer. *Nature*, 441(7097), 1068-1074.
53. Motlagh, D., Senyo, S. E., Desai, T. A., & Russell, B. (2003). Microtextured substrata alter gene expression, protein localization and the shape of cardiac myocytes. *Biomaterials*, 24(14), 2463-2476.
54. Mozaffarian D, Benjamin EJ, Go AS, et al. Heart Disease and Stroke Statistics—2015 Update: A Report From the American Heart Association. *Circulation*. January 27, 2015 2015;131(4):e29-e322.
55. Nemir, S., Hayenga, H. N., & West, J. L. (2009). PEGDA hydrogels with patterned elasticity: novel tools for the study of cell response to substrate rigidity. *Biotechnology and bioengineering*, 105(3), 636-644.
56. Nemir, S., & West, J. L. (2010). Synthetic materials in the study of cell response to substrate rigidity. *Annals of biomedical engineering*, 38(1), 2-20.
57. Norman, J. J., Mukundan, V., Bernstein, D., & Pruitt, B. L. (2008). Microsystems for biomechanical measurements. *Pediatric research*, 63(5), 576-583.

58. Pelham, R. J., & Wang, Y. L. (1997). Cell locomotion and focal adhesions are regulated by substrate flexibility. *Proceedings of the National Academy of Sciences*, 94(25), 13661-13665.
59. Pi Y, Walker JW. Diacylglycerol and fatty acids synergistically increase cardiomyocyte contraction via activation of PKC. *Am J Physiol Heart Circ Physiol*. 2000 Jul;279(1):H26-34.
60. Pieske, B., Kretschmann, B., Meyer, M., Holubarsch, C., Weirich, J., Posival, H., ... & Hasenfuss, G. (1995). Alterations in intracellular calcium handling associated with the inverse force-frequency relation in human dilated cardiomyopathy. *Circulation*, 92(5), 1169-1178.
61. Pirani, A., Vinogradova, M. V., Curmi, P. M., King, W. A., Fletterick, R. J., Craig, R., ... & Lehman, W. (2006). An Atomic Model of the Thin Filament in the Relaxed and Ca^{2+} Activated States. *Journal of molecular biology*, 357(3), 707-717.
62. Pruyne, D., Evangelista, M., Yang, C., Bi, E., Zigmond, S., Bretscher, A., & Boone, C. (2002). Role of formins in actin assembly: nucleation and barbed-end association. *Science*, 297(5581), 612-615.
63. Rajan, S., Ahmed, R. P., Jagatheesan, G., Petrashevskaya, N., Boivin, G. P., Urboniene, D, Wieczorek, D. F. (2007). Dilated cardiomyopathy mutant tropomyosin mice develop cardiac dysfunction with significantly decreased fractional shortening and myofilament calcium sensitivity. *Circulation research*, 101(2), 205-214.
64. Reilly, G. C.; Engler, A. J. Intrinsic Extracellular Matrix Properties Regulate Stem Cell Differentiation. *J. Biomech*. 2010, 43, 55–62.

65. Ribeiro, A. J., Zaleta-Rivera, K., Ashley, E. A., & Pruitt, B. L. (2014). Stable, covalent attachment of laminin to microposts improves the contractility of mouse neonatal cardiomyocytes. *ACS applied materials & interfaces*, 6(17), 15516-15526.
66. Robia SL, Ghanta J, Robu VG, Walker JW. Localization and kinetics of protein kinase C-epsilon anchoring in cardiac myocytes. *Biophys J*. 2001 May;80(5):2140-51
67. Russell, B., Curtis, M. W., Koshman, Y. E., & Samarel, A. M. (2010). Mechanical stress-induced sarcomere assembly for cardiac muscle growth in length and width. *Journal of molecular and cellular cardiology*, 48(5), 817-823.
68. Samarel, A. M. (2005). Costameres, focal adhesions, and cardiomyocyte mechanotransduction. *American Journal of Physiology-Heart and Circulatory Physiology*, 289(6), H2291-H2301.
69. Shen, Y. T., Malik, F. I., Zhao, X., Depre, C., Dhar, S. K., Abarzúa, P., ... & Vatner, S. F. (2010). Improvement of cardiac function by a cardiac myosin activator in conscious dogs with systolic heart failure. *Circulation: Heart Failure*, 3(4), 522-527.
70. Seidman, C. E., & Seidman, J. G. (2011). Identifying Sarcomere Gene Mutations in Hypertrophic Cardiomyopathy A Personal History. *Circulation Research*, 108(6), 743-750.
71. Sniadecki, N. J., & Chen, C. S. (2007). Microfabricated silicone elastomeric post arrays for measuring traction forces of adherent cells. *Methods in cell biology*, 83, 313-328.
72. Solaro, R. J., & Rüegg, J. C. (1982). Stimulation of Ca⁺⁺ binding and ATPase activity of dog cardiac myofibrils by AR-L 115BS, a novel cardiotonic agent. *Circulation research*, 51(3), 290-294.

73. Spudich, J. A. (2001). The myosin swinging cross-bridge model. *Nature Reviews Molecular Cell Biology*, 2(5), 387-392.
74. Starling, E. H. (1920). On the circulatory changes associated with exercise. *J Roy Army Med Corps*, 34, 258-72.
75. Strait, J.B., III, J.L. Martin, A. Bayer, R. Mestril, D.M. Eble, and A.M. Samarel. 2001. Role of protein kinase C-epsilon in hypertrophy of cultured neonatal rat ventricular myocytes. *Am. J. Physiol. Heart Circ. Physiol.* 280:H756–H766.
76. Sun N, Panetta NJ, Gupta DM, et al. Feeder-free derivation of induced pluripotent stem cells from adult human adipose stem cells. *Proceedings of the National Academy of Sciences*. September 15, 2009 2009;106(37):15720-15725.
77. Sun, N., Yazawa, M., Liu, J., Han, L., Sanchez-Freire, V., Abilez, O. J., ... & Wu, J. C. (2012). Patient-specific induced pluripotent stem cells as a model for familial dilated cardiomyopathy. *Science translational medicine*, 4(130), 130ra47-130ra47.
78. Takahashi, K; Yamanaka, S (2006). "Induction of pluripotent stem cells from mouse embryonic and adult fibroblast cultures by defined factors". *Cell* 126 (4): 663–76.
79. Takai Y, Kishimoto A, Inoue M, Nishizuka Y. Studies on a cyclic nucleotide-independent protein kinase and its proenzyme in mammalian tissues. I. Purification and characterization of an active enzyme from bovine cerebellum. *J Biol Chem*. 1977 Nov 10;252(21):7603-9.
80. Takeishi Y, Ping P, Bolli R, Kirkpatrick DL, Hoit BD, Walsh RA. Transgenic overexpression of constitutively active protein kinase C epsilon causes concentric cardiac hypertrophy. *Circ Res*. 2000 Jun 23;86(12):1218-23.

81. Tardiff, J. C. (2011). Thin Filament Mutations Developing an Integrative Approach to a Complex Disorder. *Circulation Research*, 108(6), 765-782.
82. Williams, C. D., Salcedo, M. K., Irving, T. C., Regnier, M., & Daniel, T. L. (2013). The length–tension curve in muscle depends on lattice spacing. *Proceedings of the Royal Society B: Biological Sciences*, 280(1766), 20130697.
83. Wingard, C. J., Browne, A. K., & Murphy, R. A. (1995). Dependence of force on length at constant cross-bridge phosphorylation in the swine carotid media. *The Journal of Physiology*, 488(3), 729-739.
84. Yamashita A, Maeda K, Maeda Y. Crystal structure of CapZ: structural basis for actin filament barbed end capping. *EMBO J*. 2003 Apr 1;22(7):1529-38. Yang WM, Tsai SC, Wen YD, Fejer G, Seto E. Functional domains of histone deacetylase-3. *J Biol Chem*. 2002 Mar 15;277(11):9447-54.
85. Yang, L., Soonpaa, M. H., Adler, E. D., Roepke, T. K., Kattman, S. J., Kennedy, M., ... & Keller, G. M. (2008). Human cardiovascular progenitor cells develop from a KDR+ embryonic-stem-cell-derived population. *Nature*, 453(7194), 524-528.

VI. Appendix

- A. Animal Care Approval Form
- B. Recombinant DNA Approval Form
- C. Curriculum Vitae

September 18, 2013

Brenda Russell Physiology &
Biophysics M/C 901

Dear Dr. Russell:

Office of Animal Care and
Institutional Biosafety Committees
(MC 672) Office of the Vice Chancellor
for Research
206 Administrative Office Building
1737 West Polk Street
Chicago, Illinois 60612-7227

The protocol indicated below was reviewed at a convened ACC meeting in accordance with the Animal Care Policies of the University of Illinois at Chicago on **9/17/2013**. *The protocol is approved for a period of 3 years with annual continuation.*

Title of Application: Isolation of Heart Cells from Neonatal Rats

ACC Number: 13-146

Initial Approval Period: 9/17/2013 to 9/17/2014

Current Funding: *Portions of this protocol are supported by the funding sources indicated in the table below.*

Number of funding sources: 2

Funding Agency	Funding Title			Portion of Funding Matched
<i>NIH</i>	<i>Integrated Mechanisms Of Cardiac Maladaptation</i>			<i>Protocol is linked to form G 13-055</i>
Funding Number	Current Status	UIC PAF NO.	Performance Site	Funding PI
<i>PO1HL62426</i> <i>(Years 11-15)</i>	<i>Funded</i>	<i>2009-06478</i>	<i>UIC</i>	<i>John Solaro (Brenda Russell, PI of project 2)</i>
Funding Agency	Funding Title			Portion of Funding Matched
<i>AHA- American Heart Association</i>	<i>Regulation of Actin Assembly in Cardiomyocytes with Mechanical Stimulation</i>			<i>All matched</i>
Funding Number	Current Status	UIC PAF NO.	Performance Site	Funding PI
<i>12PRE12050371</i>	<i>Funded</i>	<i>2012-03610</i>	<i>UIC</i>	<i>Ying-Hsi Lin</i>

This institution has Animal Welfare Assurance Number A3460.01 on file with the Office of Laboratory Animal Welfare, NIH. **This letter may only be provided as proof of IACUC approval for those specific funding sources listed above in which all portions of the grant are matched to this ACC protocol.**

Thank you for complying with the Animal Care Policies and Procedures of the UIC.

Sincerely,



Bradley Merrill, PhD
Chair, Animal Care Committee

BM/kg
cc: BRL, ACC File, Ying Hsi Li

March 9, 2015

Brenda Russell
Physiology & Biophysics
M/C 901

Dear Dr. Russell:

Office of Animal Care and
Institutional Biosafety Committees (MC 672)
Office of the Vice Chancellor for Research 206
Administrative Office Building
1737 West Polk Street
Chicago, Illinois 60612-7227

The protocol indicated below has been reviewed in accordance with the Institutional Biosafety Committee Policies of the University of Illinois at Chicago on 2/12/2015. *The protocol was not initiated until final clarifications were reviewed and approved on 3/6/2015. Protocol expires 3 years from the date of review (2/12/2018). This protocol replaces protocol 12-009 which has been terminated.*

Title of Application: Gene Expression in Muscle Using Adenoviral-Mediated Gene Transfer

IBC Number: 15-002

Highest Biosafety Level: 2

Condition of Approval: The enclosed report indicates the training status for bloodborne pathogen (BBP) training. Only those personnel who have been trained and whose training has not expired are approved for work that may involve exposure to bloodborne pathogens. Please note that federal regulations require yearly training for BBP.

You may forward this letter of acceptable IBC verification of your research protocol to the funding agency considering this proposal. **Please be advised that investigators must report significant changes in their research protocol to the IBC office via a letter addressed to the IBC chair prior to initiation of the change. If a protocol changes in such a manner as to require IBC approval, the change may not be initiated without IBC approval being granted.**

Thank you for complying with the UIC's Policies and Procedures.

Sincerely,



Randal C. Jaffe, Ph.D.
Chair, Institutional Biosafety Committee

RCJ/mbb

Enclosures

Cc: IBC file

Education

University of Illinois at Chicago

August 2013- Present

Master of Science in Bioengineering

Grade Point Average: 3.6

Georgia Institute of Technology

Fall 2009- August 2013

Bachelor of Science in Biomedical Engineering

Certificate in Social Psychology

Research

Master's Thesis Research- University of Illinois at Chicago

January 2014 – Present

Advisor: Dr. Brenda Russell

Thesis Title: Subcellular Mechanics Regulates Structure and Function of Neonatal and Stem Cell Derived Cardiomyocytes

Research focuses on assessing structure and function of cardiac cells. Study involves static loading of myocytes to determine changes in contractility and sarcomere assembly. Static loads were simulated by life-like 3D anchorage for the single cell analysis of contractile and actin remodeling. The second part of this study involves cardiomyocytes derived from induced pluripotent stem cells (iPSC-CMs) from affected patients that carried a cTnT R173W point mutation to examine their functional characteristics during early and late development, as compared to iPSC-CMs from normal family members. The cells were also treated with 200 nM dose of a calcium sensitizing drug, Omecamtiv Mecarbil, to test whether this drug could therapeutically rescue the mutation cells during its development stage to a normal physiological range.

Capstone Design-Georgia Tech

January 2013 – May 2013

Senior Design Research. Redesigned surgical instruments for a plastic surgery instrument kit specialized for a blepharoplasty procedure. Instruments were designed to improve ergonomics and function. Prototypes were constructed using various 3D Printers, including MakerBot.

Cellular Biomechanics Laboratory- Georgia Tech

January 2012-August 2012

Research focused on adhesion and signaling molecules involved in processes of inflammation, hemostasis, and T-cell activation. To study the mechanics and kinetics of cell and molecular interactions, an image analysis system was developed to detect the adhesion of T-cells to red blood cells.

Laboratory of Neuroengineering- Georgia Tech

September 2010- February 2011

Research focused on imaging cultured mammalian neurons to study learning and neural processing in vitro. Project consisted of constructing and improving a device that manages temperature and gas partial pressures within an insulated microscope enclosure, allowing the imaging of neuronal cell cultures for extended time periods.

Work Experience

Commercialization and Strategy Consultant for EnterpriseWorks Chicago

February 2014-December 2014

EnterpriseWorks incubator is owned and operated by the University of Illinois to help launch successful startup companies in the biotechnology field. Tasks include aiding in technology commercialization development with inventors of biotechnology startup companies to move novel innovations into the marketplace

Bioscience Intern for Metro Atlanta Chamber

May-August 2012

Aided in execution of market research initiatives of the Medical Device Subcommittee, including setting up a database, creating reports and conducting primary and secondary research of various companies

Research Intern for Neural Signals, Inc.

May-August 2011

Research focused on invasive brain computer/machine interfacing with regards to speech restoration. Project consisted of analyzing data obtained from neural recordings with an electrode implanted into the cerebral cortex in a mute and paralyzed subject during attempts at inner speech to determine if the detected beta-band peaks of the neural signal correlated with the onset of silent speech.

Publications

Sarmah E, Kennedy P. "Detecting Silent Vocalizations in a Locked-In Subject". *Neuroscience Journal*. 2013; Hindawi Publishing Corporation 2013:12.

Skills

Programming Languages: MATLAB, Python, LabVIEW

Software: Microsoft Office Suite, Solidworks, NeuroExplorer and NeuroLynx

Laboratory: Cell Culture, Confocal Microscopy, Immunofluorescent Staining

Professional Skills: Technical writing, public speaking/presentation skills, collaborative work, and creative problem solving

Languages: Assamese (Native), Spanish (Intermediate Proficiency)

Involvement

Society of Women Engineers

August 2013 – Present

Member of SWE Chicago Regional Section, which is a non-profit group that encourages women to pursue their passions in STEM fields

Georgia Institute of Technology Vibha-Atlanta, GA

Student led organization that promotes awareness about and fundraises to support the education and welfare of underprivileged children.

Volunteer Chairperson and Event Committee Chair,

August 2010- May 2013

Lead the committee in developing, executing and updating the action plan for various fundraising events. Conducted membership recruitment activities and membership retention activities as well as membership campaigns

Pioneer – Biomedical Engineering Newsletter, Georgia Tech

Wallace H. Coulter Department student newsletter of Georgia Tech and Emory University

Editor and Writer, August 2010- April 2012

Oversaw newsletter deadlines. Planned, organized, edited and wrote parts of the content of each month's newsletter.